NeuroImage 201 (2019) 116000

Contents lists available at ScienceDirect

NeuroImage

journal homepage: www.elsevier.com/locate/neuroimage

Using machine learning-based lesion behavior mapping to identify anatomical networks of cognitive dysfunction: Spatial neglect and attention

Daniel Wiesen [a], Christoph Sperber [a], Grigori Yourganov [b], Christopher Rorden [b], Hans-Otto Karnath [a,b,*]

[a] Center of Neurology, Division of Neuropsychology, Hertie-Institute for Clinical Brain Research, University of Tübingen, Tübingen, 72076, Germany
[b] Department of Psychology, University of South Carolina, Columbia, 29208, USA

ARTICLE INFO

Keywords:
Stroke
Spatial attention
Support vector regression
VLSM
Voxel-based lesion behavior mapping
Multivariate

ABSTRACT

Previous lesion behavior studies primarily used univariate lesion behavior mapping techniques to map the anatomical basis of spatial neglect after right brain damage. These studies led to inconsistent results and lively controversies. Given these inconsistencies, the idea of a wide-spread network that might underlie spatial orientation and neglect has been pushed forward. In such case, univariate lesion behavior mapping methods might have been inherently limited in detecting the presumed network due to limited statistical power. By comparing various univariate analyses with multivariate lesion-mapping based on support vector regression, we aimed to validate the network hypothesis directly in a large sample of 203 newly recruited right brain damaged patients. If the exact same correction factors and parameter combinations (FDR correction and dTLVC for lesion size control) were used, both univariate as well as multivariate approaches uncovered the same complex network pattern underlying spatial neglect. At the cortical level, lesion location dominantly affected the temporal cortex and its borders into inferior parietal and occipital cortices. Beyond, frontal and subcortical gray matter regions as well as white matter tracts connecting these regions were affected. Our findings underline the importance of a right network in spatial exploration and attention and specifically in the emergence of the core symptoms of spatial neglect.

1. Introduction

Spatial attention and orientation is a cognitive function dominantly represented in the human right hemisphere (Corbetta et al., 2008, 2005). In correspondence, spatial neglect is one of the most common syndromes after brain injury of predominantly this hemisphere (Stone et al., 1993; Becker and Karnath, 2007; Ten Brink et al., 2017). Patients spontaneously and sustainably deviate towards the ipsilesional side, neglecting contralesionally located information or stimuli (Heilman et al., 1983; Karnath and Rorden, 2012). The anatomical basis of this core deficit of spatial neglect has been extensively investigated using mass-univariate lesion behavior mapping methods (VLBM), such as VLSM (Bates et al., 2003) or NPM (Rorden et al., 2007). Heterogeneous findings were observed, causing lively controversies (for review Karnath and Rorden, 2012). In the right hemisphere, spatial neglect has been reported to be associated with parietal lesions to regions in the inferior parietal lobule and temporo-parietal junction (Chechlacz et al., 2010; Karnath et al., 2011; Rousseaux et al., 2015), the superior and middle temporal cortex as well as the insula (Karnath et al., 2004, 2011; Committeri et al., 2007; Sarri et al., 2009; Chechlacz et al., 2010; Saj et al., 2012; Rousseaux et al., 2015) and the ventrolateral prefrontal cortex (Committeri et al., 2007; Thiebaut De Schotten et al., 2014). These cortical areas were also found to be involved in the human left hemisphere when patients show spatial neglect after a left hemisphere stroke (Suchan and Karnath, 2011). Furthermore, disrupted structural connectivity has been related to spatial neglect, including damage of the superior longitudinal fasciculus and arcuate fasciculus, the inferior occipito-frontal fasciculus, extreme capsule and the superior occipito-frontal fasciculus, as well as the middle longitudinal fasciculus (Thiebaut de Schotten et al., 2005; He et al., 2007; Urbanski et al., 2008, 2011; Karnath, 2009; Shinoura et al., 2009; Ciaraffa et al., 2013; Thiebaut De Schotten et al., 2014; Umarova et al., 2014; Vaessen et al., 2016; Carter et al., 2017; de Haan and Karnath, 2017).

Abbreviations: VLBM, Voxel-based lesion behavior mapping; MLBM, Multivariate lesion behavior mapping; SVR, Support vector regression; SVR-LSM, Support vector regression based lesion-symptom mapping; FDR, false discovery rate; FWE, Family Wise Error; dTLVC, Direct Total Lesion Volume Control.

* Corresponding author. Center of Neurology, University of Tübingen, 72076, Tübingen, Germany.
E-mail address: karnath@uni-tuebingen.de (H.-O. Karnath).

https://doi.org/10.1016/j.neuroimage.2019.07.013
Received 21 February 2019; Received in revised form 2 July 2019; Accepted 4 July 2019
Available online 9 July 2019

Hence, building on the seminal work by Watson et al. (1974) and Mesulam (1981), it has been concluded in review articles (Catani, 2006; Bartolomeo et al., 2007; Karnath, 2009; Karnath and Rorden, 2012; Lunven and Bartolomeo, 2017) and meta-analyses (Chechlacz et al., 2012; Molenberghs et al., 2012) that an anatomical network (Karnath, 2009; Karnath and Rorden, 2012) might represent the basis of spatial neglect.

Part of the heterogeneity in the anatomical correlates of spatial neglect may be determined by the fact that the different studies were varying largely in the application of different analysis procedures and methodological choices, including e.g. statistical tests, statistical thresholding, corrections for multiple comparisons, or procedures for lesion volume control. In fact, statistical lesion behavior mapping approaches provide many degrees of freedom and pitfalls to a researcher (for review, see Sperber and Karnath, 2018). Beyond, the statistical analysis techniques themselves each come along with specific strength and weaknesses. For example, traditional mass-univariate lesion behavior mapping methods can be ill-suited in situations, where lesions of multiple brain areas contribute to a pathological behavior. Due to the so-called 'partial injury problem' (Rorden et al., 2009; Sperber et al., 2019), statistical power of VLBM in anatomical networks might be reduced, and false negative findings might conceal the full network. This issue has been confirmed by several simulation studies (Mah et al., 2014; Zhang et al., 2014; Pustina et al., 2018). Furthermore, the huge number of independent tests in VLBM as well as in some of the multivariate lesion behavior mapping (MLBM) implementations requires control for multiple comparisons, which can further reduce statistical power. This might have contributed to the heterogeneous pattern of previous results in spatial neglect, with different studies identifying some nodes while missing others. Additional facts which can explain heterogeneous anatomical findings might be based on the specific sample characteristics in previous investigations (Gajardo-Vidal et al., 2018). The authors showed that specific sub-sets of patients can drive significant results. This might be especially true in smaller studies with lower power (Lorca-Puls et al., 2018).

Unlike VLBM's mass-univariate testing approach, machine learning based lesion analysis offers a multivariate approach to lesion analysis. Multivariate lesion behavior mapping (MLBM) appears to be particularly suitable to identify neural correlates of behavior organized in networks (Smith et al., 2013; Mah et al., 2014; Zhang et al., 2014; Yourganov et al., 2015; Zavaglia and Hilgetag, 2016; Pustina et al., 2018; for review Karnath et al., 2018). Two recent studies investigated the neural correlates of spatial neglect with MLBM, one using support vector machines in a sample of 140 right hemisphere stroke patients (Smith et al., 2013), the other a game theoretical approach in a small sample of only 25 (and even less for subtests) right hemisphere patients (Toba et al., 2017). Both studies had limitations. The two approaches were constrained to the investigation of only a few brain regions at once, in other words, these approaches did not provide a voxel-by-voxel analysis of the lesion pattern throughout the brain. Moreover, regions in such region-based approaches can differ both from the relevant functional parcellation of the brain and the typical anatomy of stroke lesions and thus might have failed to capture relevant brain regions. In contrast, Support Vector Regression based Multivariate Lesion-Symptom Mapping (SVR-LSM) utilizes voxel-wise whole brain information independently of an a priori region of interest selection (Zhang et al., 2014). Different groups have recently validated and tested this approach (Zhang et al., 2014; DeMarco and Turkeltaub, 2018; Sperber et al., 2019).

Further, we assume that part of the apparent diversity in previous anatomical results reflects small sample sizes used in part of the previous studies. Moreover, many prior studies have treated neglect as a categorical deficit, whereas there is clear evidence that the symptom severity varies between individuals (Rorden and Karnath, 2010). Likewise, some prior studies have measured attentional deficits that dissociate from each other (Karnath and Rorden, 2012). If these sources of variability in impairment correlate with the location and extent of injury, studies that treat neglect as merely present or absent may suffer further reduced power. Therefore, the aim of the present study is to use anatomical data from a large sample of 203 newly recruited right hemisphere damaged patients in order to apply and compare several univariate VLBM techniques as well as the multivariate SVR-LSM method (Zhang et al., 2014) to identify the anatomical representation underlying spatial neglect. For the comparison of methods, we focus especially on those VLBM techniques that correspond to the majority of the current univariate lesion-mapping studies (for review, see de Haan and Karnath, 2018), addressing a cross-section of statistical thresholding methods and procedures for lesion volume control.

Moreover, in order to reduce the possible influence of different symptoms of and clinical tests for spatial neglect, we here focus on only the egocentric core component of spatial neglect (see Karnath and Rorden, 2012), using a continuous measure to capture symptom severity. This core component is represented by a spontaneous and sustained deviation of eyes and head towards the ipsilesional side (Fruhmann-Berger and Karnath, 2005; Fruhmann-Berger et al., 2006; Becker and Karnath, 2010), combined with neglect of contralesionally located information or stimuli. This spatial bias can be reliably measured amongst others by traditional cancellation tasks (Rorden and Karnath, 2010) as well as a modified line bisection task (McIntosh et al., 2017). As noted, several spatial and non-spatial attentional symptoms that have been associated with neglect patients (e.g. Binder et al., 1992; Husain et al., 1997; Barton and Black, 1998; Ferber and Karnath, 2001; Azouvi, 2002; Husain and Rorden, 2003; Verdon et al., 2010; Sperber et al., 2016; McIntosh et al., 2017), though many of these symptoms can dissociate both anatomically and behaviorally. Our goal was to have a robust and pure measure for the core spatial bias, uncontaminated by these other symptoms.

2. Materials and methods

2.1. Subjects

Neurological patients consecutively admitted to the Center of Neurology at Tuebingen University were screened for a first ever right-hemisphere stroke. Patients with a left-sided stroke, patients with diffuse or bilateral brain lesions, patients with tumors, as well as patients in whom MRI or CT scans revealed no obvious lesions were not included. In total 203 patients were recruited in the acute phase after stroke (3.2 and 4.2 days post-stroke on average; cf. Table 1). None of these patients were included in any of our previous studies addressing the anatomy of spatial neglect (Karnath et al., 2001, 2004; 2011; Smith et al., 2013). Therefore, they represent an independent, new sample. Table 1 gives the demographic and clinical data. All subjects provided written informed consent and the study was conducted in accordance with the ethical guidelines from the revised Declaration of Helsinki and in accordance with relevant guidelines and regulations.

2.2. Behavioral examination

The interval between stroke-onset and neuropsychological examination was maximally 25 days (mean = 4.37 days, SD = 4.04). The following neuropsychological tests were performed: Letter Cancellation Task (Weintraub and Mesulam, 1985) and Bells Test (Gauthier, Louise Dehaut, Francois Joanette, 1989). These two tests were presented on a horizontally oriented 21 × 29.7 cm sheet of paper which was fixed at the center of the patient's sagittal midline. In the Letter Cancellation task, 60 target letters 'A' are distributed among other distractor letters. The Bells test requires identifying 35 bell icons distributed all over the sheet between other symbols. In these two cancellation tasks, patients were asked to cancel all of the targets, 'A' letters or bells respectively. The maximum duration of each test was not fixed in advance but depended on the patient being satisfied with his performance and confirming this twice. For the Letter and Bells Cancellation tasks, we calculated the Center of Cancellation (CoC) using the procedure by Rorden and Karnath (2010).

The CoC is a sensitive measure capturing both the number of omissions, as well their location. For the lesion behavior mapping, we calculated the mean CoC from the two cancellation tasks for each patient and used this score for our analyses. Visual field defects were examined by the common neurological confrontation technique.

2.3. Imaging

Structural imaging was acquired either by MRI (n = 106) or CT (n = 97), performed on average 3.5 days (SD = 4.6) after stroke-onset. If both imaging modalities were available, MR scans were preferred. In participants where MR scans were available, we used diffusion-weighted imaging (DWI) if the images were acquired within 48 h after stroke onset or T2-weighted fluid attenuated inversion recovery (FLAIR) images for later scans. Lesion boundaries were manually marked on the transversal slices of the individual MR or CT scans using the free MRIcron software (www.mccauslandcenter.sc.edu/mricro/mricron).

Normalization of CT or MR scans to MNI space with 1x1x1 mm resolution was performed by using the Clinical Toolbox (Rorden et al., 2012) under SPM8 (www.fil.ion.ucl.ac.uk/spm), and by registering lesions to its age-specific templates oriented in MNI space for both CT and MR scans (Rorden et al., 2012). If available, the MR scans were co-registered with a high resolution T1-weighted structural scan in the normalization process. Delineation of lesion borders and quality of normalization were verified by consensus of always two experienced investigators (one of them H.-O.K.). An overlap of all normalized lesions is shown in Fig. 1. The average lesion size in the sample was 45.52 cm^3 (SD = 52.67 cm^3). In the supplemental material we show overlap plots of normalized lesions separated for each imaging modality (Fig. S1) as well as a histogram of the lesion size distribution (Fig. S2 B). Moreover, we provide a figure showing the regional bias caused by lesion volume (Fig. S3).

2.4. Multivariate lesion behavior mapping

2.4.1. Support vector regression

For our analysis, we implemented a multivariate lesion-symptom mapping method based on support vector regression (SVR) (Drucker et al., 1996; Vapnik, 1995). Lesion mapping based on support vector regression employs supervised machine learning algorithms to develop a model based on training input data which best describes the continuous relationship between behavioral scores and lesion location. Hence, it can be seen as an extension of Support Vector Machines (SVM) (Cortes and Vapnik, 1995) used for classifying data sets into different categories. Support vector regression based lesion-symptom mapping (SVR-LSM) has already been implemented and validated in a synthetic dataset, in a real dataset composed of aphasic patients (Zhang et al., 2014), as well as several recent publications (Xing et al., 2015; Fama et al., 2017; Griffis et al., 2017a,b; Lacey et al., 2017; Skipper-Kallal et al., 2017; Chen et al., 2018; DeMarco and Turkeltaub, 2018; Zhao et al., 2018; Sperber et al., 2019).

Table 1
Demographic and clinical data of the 203 patients included.
For this table we determined whether a CoC (= Center of Cancellation; see Rorden and Karnath, 2010) score was in the pathological range; cut-offs were set at >0.081 for the Bells Cancellation Task and >0.083 for the Letter Cancellation test (cf. Rorden and Karnath, 2010). In order to assign the diagnosis of spatial neglect, patients had to present a pathological test score in at least one of the two cancellation tests. Using this criterion, 81 (40%) were classified as exhibiting spatial neglect while 122 (60%) did not exhibit neglect. Data are represented as mean (SD). Note that in the statistical tests we treated neglect severity as a continuous measure. The table reveals that using cut-off thresholds, there is little variability in patients without pathological bias (ceiling performance), while symptom severity varies across patients with pathological deficits.

	Neglect	No neglect
Age (years)	64.7 (12.4)	60.2 (13.7)
Sex (M/F)	48/33	71/51
Etiology (Ischemia/Hemorrhage)	69/12	104/18
Lesion size (cm^3)	70.0 (64.4)	29.3 (35.0)
Time since lesion (days)	4.2 (4.3)	3.2 (4.5)
Letter Cancellation (CoC)	0.36 (0.32)	0.01 (0.02)
Bells Cancellation (CoC)	0.39 (0.29)	0.01 (0.03)
Visual Field Defects (% present)	27	14
Imaging (CT/MRI)	44/37	53/69

Data Analysis. The analysis was performed with MATLAB 2016a and libSVM Vers. 3.21 (Chang and Lin, 2013). We used a publicly available collection of scripts (https://github.com/yongsheng-zhang/SVR-LSM) employed in the study by Zhang et al. (2014) and adopted algorithms for control for lesion size and for the derivation of a topography from SVR β-parameters. For the detailed methodological procedure and theoretical background of SVR-LSM in general, see Zhang et al. (2014). Only voxels where at least 10 patients had a lesion were included in the analysis and constituted the voxel mask for statistical testing. Exclusion of voxels with infrequent lesion affection was performed to restrict the analysis to voxels with reasonable statistical power and thus to reduce the potential that the results are biased by brain regions that are only rarely affected (Karnath et al., 2018). The employed analysis is therefore no strict whole-brain analysis, but – contrary to region-of-interest analyses – it allows an investigation of all brain areas that contain a certain degree of information. First, the lesion status of each participant was regrouped into a column vector. To control for lesion size, each vector was then normalized to have a unit norm, a procedure also known as direct total lesion volume control (dTLVC) (Zhang et al., 2014). Lesion volume control is an important preprocessing step as the severity of a symptom is generally related to the lesion size, as shown for our data ($r = 0.54$; $p < 0.001$) in Fig. S2 A in the supplemental material. To ensure, that this latter correlation is not solely driven by a few patients having very large lesions >150 cm^3, we further report the correlation for the subset of patients having lesions <150 cm^3 (N = 195). Although the strength of the association decreases to some degree, lesion size stays significantly related to the severity of the spatial neglect behavior ($r = 0.43$; $p < 0.001$). To estimate the SVR hyperplane and project our initial data into a higher dimensional space, we implemented an epsilon-SVR model and used a non-linear radial basis function (RBF) Kernel. In order to improve the performance of the learning algorithms and to choose a model best describing our data, a preselection of the model hyper-parameters cost (C) and gamma (γ) needs to be done. Following general recommendations in the libSVM toolbox manual (Chang and Lin, 2013), we added an optimization procedure using grid search. The range of investigated parameters was chosen as in the study by Zhang et al. (2014): C = 1, 10, 20, 30, 40, 50, 60, 70, 80, and γ = 0.1, 1, 2, 3, 4, 5, 6, 7, 8, 9, 10, 15, 20, 25, 30. Using a five-fold cross-validation scheme, we evaluated both prediction accuracy and reproducibility of each parameter combination (see Zhang et al., 2014). During this procedure, the whole dataset is separated into 4/5 training data, which is used to generate the multivariate model. Then this model is tested on the unknown leftover 1/5 of the data to prevent overfitting and to get a good estimate of the performance of the model to unknown data. To save computational power, we reduced the number of iterations from 40 to 5 compared to the initial analysis in Zhang et al. (2014) and evaluated mean prediction accuracy and reproducibility scores, based on these 5 iterations for each parameter set. We define mean prediction accuracy, as in Zhang et al. (2014), to be the mean correlation coefficient between predicted scores and out of sample testing scores of 5 times 5-fold cross-validations. Note that for each of the 5 iterations, new random subsets of training and testing scores were drawn from the whole dataset. After SVR model construction, β-parameters are remapped onto a three-dimensional brain topography allowing us to derive the reproducibility score by calculation of the mean correlation coefficient between any two SVR-LSM β-parameter maps from the drawn subsets. Finally, using the best combination of C and γ for model construction, the remapped β-parameters are tested by using a permutation approach,

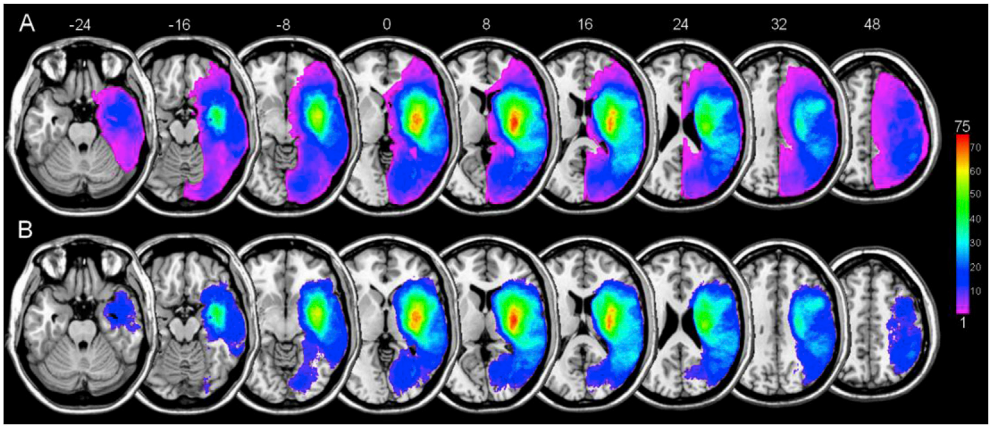

Fig. 1. Topography of brain lesions. A: Simple lesion overlap topography of all 203 patients. **B:** Lesion overlap topography showing only voxels within the voxel mask for statistical testing with at least 10 patients having a lesion. The colorbar indicates the number of overlapping lesions (the peak of N = 75 represents 37% of the total sample). Numbers above the slices indicate z-coordinates in MNI space.

comparing the SVR β-parameters voxel-wise with new β-parameters drawn for each permutation through randomization of behavioral scores. Results are reported with correction for multiple comparisons that survived a False Discovery Rate (Benjamini and Yekutieli, 2001) (FDR) correction at $q = 0.05$, determined by 10000 permutations. As statistical testing is performed on a voxel-by-voxel basis, a form of multiple comparison correction is required to prevent an increase of false alarms (Sperber et al., 2019).

2.5. Univariate voxel-based lesion behavior mapping

To compare the SVR-LSM technique with traditional analyses, we also performed mass-univariate VLBM analyses on the same data set. As for MLBM, only voxels where at least 10 patients had a lesion were included in the analysis and constituted the voxel mask for statistical testing. The variants of lesion volume correction and correction for multiple comparisons differ between univariate studies. Nevertheless, the exact choice might have an impact on the topographical outcome of the univariate results, as shown recently by Pustina et al. (2018). Therefore, we decided to show results using different parameter configurations, providing a small cross section of what is currently employed in the field. Hence, for the univariate analyses, there were in total 4 configurations: A) without correction for lesion size including family-wise error correction (FWE) for multiple comparisons based on 10000 permutations at $p < 0.05$; B) with correction for lesion size – by regressing lesion size out of behavior – including FWE correction for multiple comparisons based on 10000 permutations at $p < 0.05$; C) without correction for lesion size including False Discovery Rate (FDR) correction for multiple comparisons at $q = 0.05$; D) with correction for lesion size – by regressing lesion size out of behavior – including FDR correction for multiple comparisons at $q = 0.05$. Finally, to increase comparability to our multivariate findings, we additionally performed one analysis with similar parameter configurations, using minimum lesion affection of 10, FDR correction for multiple comparisons at $q = 0.05$, as well as dTLVC as lesion volume control procedure.

All univariate analyses were carried out using the NiiStat tool (https://github.com/neurolabusc/NiiStat) and were based on the general linear model (identical to a Student's pooled-variance *t*-test). To get a further direct quantitative comparison between multivariate and univariate mapping models, we compared the predictive performance of both techniques using the same parameter configurations in terms of lesion volume control and minimum lesion affection. Hence, for the univariate lesion behavior mapping, we implemented a 5 times 5-fold procedure on each single voxel and derived the predictive performance in terms of R^2, using the same parameter configurations as for our main multivariate analysis. Therefore, minimum lesion affection was set to $N = 10$ and the dTLVC procedure to control for lesion volume was used. During this procedure, the whole dataset was separated into 4/5 training data, which is used to generate a univariate model for each single voxel. Subsequently, this model was tested on the unknown leftover 1/5 of the data to prevent overfitting and to get a good estimate of the performance of the model to unknown data. We then evaluated mean prediction performance in terms of R^2 based on these 5 iterations for each voxel. We defined mean prediction performance to be the mean R^2 value between predicted scores and out of sample testing scores of 5 times 5-fold cross-validations. Note that for each of the 5 iterations new random subsets of training and testing scores were drawn from the whole dataset. Finally, we evaluated if the predictive performance of the multivariate model is superior to each of the models of each single voxel when univariate mapping is used.

2.6. Supplementary analysis

While the need of lesion volume correction is widely accepted, the exact technique to be used is still under discussion. Zhang et al. (2014) validated the dTLVC method for real and synthetic lesion data and argued that a regression based correction might be excessively conservative. On the other hand, DeMarco and Turkeltaub (2018) put forward that the dTLVC method might be too liberal and advocated for using regression based correction. To address both positions and concerns, we implemented a supplemental analysis using the same parameters as for our main SVR-LSM analysis, except for now regressing lesion size out of both behavioral and lesion scores instead of the dTLVC procedure. Scripts for this supplemental analysis have been adopted from a recently published toolbox and are available online (github.com/atdemarco/svrlsmgui; DeMarco and Turkeltaub, 2018).

2.7. Atlas overlap

Labeling of all the resulting voxel-wise statistical maps with respect to grey matter brain regions was done by overlaying the maps on the Automatic Anatomical Labelling atlas (AAL; Tzourio-Mazoyer et al., 2002) distributed with MRIcron. The localization of white matter fiber tracts damaged by the lesion was based on two different fiber tract atlases: the Juelich probabilistic cytoarchitectonic atlas (Bürgel et al., 2006) as well as the tractography-based probabilistic fiber atlas (Thiebaut de Schotten et al., 2011). We decided to interpret the data according to these two WM atlases simultaneously due to the marked variance between DTI- and histology-based white matter atlases (de Haan and Karnath, 2017). The WM probabilistic maps were thresholded at $p \geq 0.3$ before being overlaid on the statistical topography.

3. Results

3.1. Parameter optimization

Testing different sets of C and γ combinations, we got a similar pattern of that what has already been reported in previous investigations (Rasmussen et al., 2012; Zhang et al., 2014). Thus, the C and γ variables provide a trade-off between prediction accuracy and reproducibility (Fig. 2 A and B). Without having any reference about a certain standard in choosing the right parameter combination, we decided to perform the final analysis with a C of 30 and γ of 4, as these values provided, compared to the other combinations, a decent prediction accuracy (0.43) while keeping the reproducibility index (0.91) as high as possible. With this combination, the model achieves an average cross-validation R^2 of 0.19, averaged over runs and folds from the repeated 5-fold cross-validation scheme. Note that these values have been drawn from the 5 times 5-fold cross-validation optimization routine and hence reflect the model performance when 4/5 of the dataset were used for model creation and 1/5 for model testing. It is worth noting that the R^2 reflects prediction after one has accounted for lesion volume (see section 2.6 above). Note that lesion volume is virtually always a strong predictor of behavior: large lesions are likely to compromise sufficient portions of distribute networks and large hubs to elicit symptoms, and larger lesions are probabilistically more likely to hit small modules than smaller injuries. Therefore, the reported R^2 are with respect to the residual variability after the strong factor is accounted for. This has clear implications for clinical prognosis, where both lesion volume and location can be leveraged.

3.2. Multivariate lesion behavior relationships

Resulting topographies of the SVR-LSM analysis using continuous CoC scores revealed a perisylvian network including parietal, frontal and temporal grey matter regions as well as clusters in WM fibers (Fig. 3). An exact overview of the grey and white matter structures significantly involved and showing at least 100 mm^3 overlapping voxels with the respective atlas structures is given in Table 2. Large clusters incorporated middle and superior temporal gyri as well as the inferior parietal lobule, including angular and supramarginal gyri. Smaller clusters affected inferior and middle frontal gyri, as well as the pre- and postcentral gyri. Moreover, significant lesion patterns included the insula and subcortical structures such as the pallidum, putamen and caudate nucleus. The overlap with both WM atlases consistently showed significant clusters affecting the uncinate fasciculus and the inferior occipito-frontal fasciculus. In addition, only the WM atlas by Thiebaut de Schotten et al. (2011) implicated the inferior longitudinal, as well as the superior longitudinal/arcuate fasciculus and the internal capsule, while only the Juelich WM atlas identified the superior occipito-frontal fasciculus. In addition, Fig. 3D the thresholded β–map of the SVR-LSM analysis is plotted, showing the association between individual voxel-wise β-weight to the behavioral score (see Sperber et al., 2019).

3.3. Univariate voxel-based lesion behavior relationships

The VLBM analysis most similar to the MLBM procedure, using FDR correction and dTLVC for lesion size control, revealed a lesion pattern which concurs largely with that of the MLBM results (Fig. 4 and Table 3A).

In contrast, the VLBM analysis including family-wise error correction (FWE) for multiple comparisons without correction for lesion size (Fig. 5A) revealed mainly involvement of inferior and middle frontal as well as middle and superior temporal cortical grey matter areas. Moreover, subcortical affection of the putamen, caudate nucleus, and pallidum was seen; no significant effects were detected in parietal cortex. A detailed overview of grey and white matter structures significantly involved and with at least 100 mm^3 overlap with the respective atlases is given in Table 3B. The comparison with white matter atlases reveals involvement of the superior occipito-frontal fasciculus for the Juelich WM atlas as well as the arcuate and uncinate fasciculi for the WM atlas by Thiebaut de Schotten et al. (2011). Moreover, the latter delineated affection of the inferior occipito-frontal and longitudinal fasciculi, as well as the internal capsule.

The VLBM analysis including family-wise error correction (FWE) and a correction for lesion size (Fig. 5B) revealed only a small cluster within frontal white matter. The univariate analysis using FDR-thresholding without correction for lesion size is showing a wide spreading map with 56% of the tested voxels becoming significant, spanning over frontal, temporal, parietal and occipital as well as subcortical areas and clusters in white matter fibres (Fig. 5C). A detailed overview of grey and white matter structures significantly involved and with at least 100 mm^3 overlap with the respective atlases is given in Table 3C. On the other side, employing lesion volume correction, the analysis with FDR-thresholding showed a rather conservative pattern – similar to FWE-thresholding with correction for lesion size – of two small clusters in the frontal white matter with no corresponding atlas label (Fig. 5D).

3.4. Quantitative comparison between univariate and multivariate lesion-behavior mapping

The comparison of the predictive performance between univariate and multivariate procedures showed that the predictive performance in terms of R^2 (cross-validation R^2, averaged over runs and folds from the repeated 5-fold cross-validation scheme) of each single voxel in univariate lesion behavior mapping yielded a maximum R^2 of 0.21. On the first

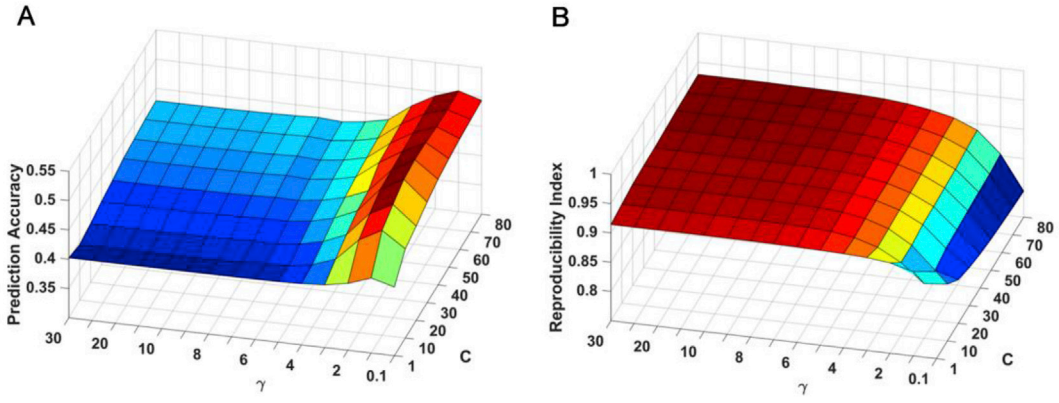

Fig. 2. Estimation of best hyper-parameters C and γ. SVR-LSM parameter estimation results. Prediction Accuracy (**A**) and Reproducibility Index (**B**) (see Rasmussen et al., 2012; Zhang et al., 2014) are plotted for the different sets of C and **γ** parameters to find the optimal combination.

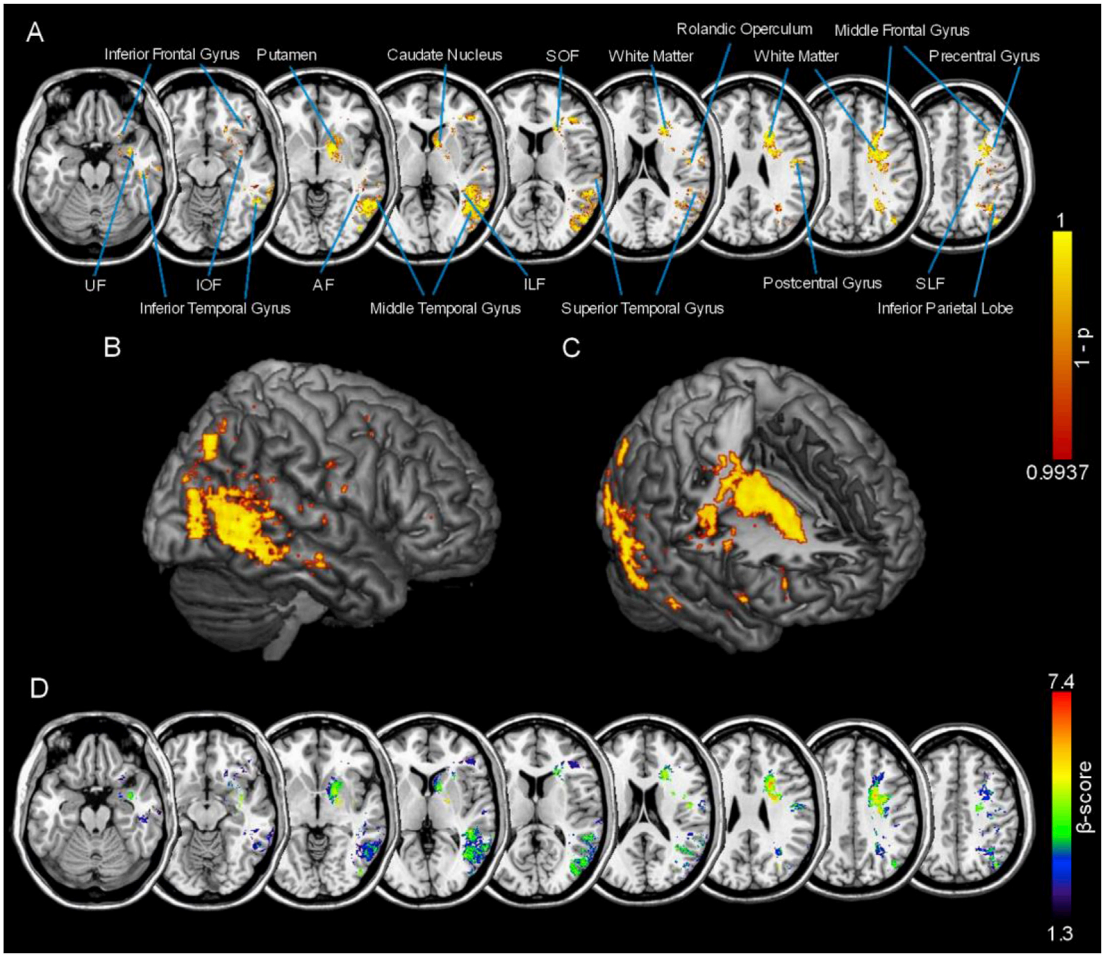

Fig. 3. Results of the multivariate lesion behavior mapping. Support vector regression based multivariate lesion-symptom mapping results using data of 203 patients. Lesion volume correction was performed by applying dTLVC. A: Permutation-thresholded statistical map of SVR-LSM on CoC scores (FDR-corrected at $q = 0.05$, corresponding to a threshold of $p < 0.0063$), illustrating the anatomical regions significantly associated with the core deficit of spatial neglect. Significant clusters were interpreted according to the AAL atlas (Tzourio-Mazoyer et al., 2002) for grey matter regions and to the Juelich probabilistic cytoarchitectonic fiber tract atlas (Bürgel et al., 2006) as well as the tractography-based probabilistic fiber atlas by Thiebaut de Schotten et al. (2011) for white matter structures. B and C: three-dimensional renderings of the same map using the 3D-interpolation algorithm provided by MRIcron (http://people.cas.sc.edu/rorden/mricron/index.html; 8 mm search depth) with sagittal view for B and inside view for C. Results of A, B and C are shown as 1-p. D: Thresholded β-parameter map showing only significant areas according to A. Abbreviations: SLF – superior longitudinal fasciculus; AF – arcuate fasciculus; ILF – inferior longitudinal fasciculus; IOF – inferior occipitofrontal fasciculus; SOF – superior occipitofrontal fasciculus; UF – Uncinate fasciculus.

sight, this seems superior to the R^2 of 0.19 – both R^2 values after correcting for lesion volume – found for multivariate mapping. Nevertheless, for univariate lesion behavior mapping only 12 voxels exceeded the R^2 of 0.19. The location of these 12 voxels corresponded spatially to the spot in frontal white matter that we obtained in all of the univariate lesion behavior mapping topographies with highest z-scores (see Fig. 5); it might reflect an area with largest power across all of our univariate analyses. On the other side, the prediction performance of all the other voxels throughout the tested area in univariate modelling was inferior to the multivariate model (all $R^2 < 0.19$). To make sure that the overall multivariate model is indeed better and the predictive performance not only driven by the same 12 voxels, which show the most predictive individual contribution in VLBM, we repeated the cross-validation scheme for SVR-LSM with exclusion of these 12 voxels. By excluding these voxels, this further evaluation results in a predictive performance of $R^2 = 0.187$ and confirms that the multivariate model is not driven by only a few single voxels. A figure showing the frequency distribution of all mass-univariate R^2 values with the location of the multivariate R^2 values including as well as excluding the 12 maximum voxels of the univariate analysis is shown in the supplement (Fig. S4).

3.5. Supplementary analysis

In a recent investigation, it has been advocated for the use of a new technique for correction for lesion size (e.g. regression of lesion volume out of both, behavior and lesion). Therefore, we implemented a supplemental analysis using the same parameters as for our main SVR-LSM analysis, except for now regressing lesion size out of both behavioral and lesion scores instead of the dTLVC procedure. The optimization procedure delineated a C of 1 and γ of 0.1 as optimal parameters revealing a prediction accuracy of −0.02 and a reproducibility index of 0.88. With this combination, the model achieves an $R^2 < 0.001$. Results for the supplemental analysis revealed a much more conservative pattern as compared to the SVR-LSM analysis with dTLVC correction. If we regress lesion size out of both behavioral and lesion scores, the resulting topographies centered on several smaller nodes (see Supplementary Material; Fig. S5). One cluster of lesion symptom associations was found within the right basal ganglia (putamen, pallidum, head of caudate nucleus). Moreover, an anterior cluster was revealed within the white matter adjacent to inferior and middle frontal gyri. A further small node was found at the right middle/inferior temporal cortex.

Table 2
Detailed overview of all significant grey and white matter clusters – MLBM. Overlap of MLBM analysis with grey and white matter atlases (FDR-corrected at $q = 0.05$, corresponding to a threshold of $p < 0.0063$). For grey matter structures, reports are generated using the Automatic Anatomical Labeling atlas (AAL; Tzourio-Mazoyer et al., 2002). For white matter structures, reports are generated using the Juelich probabilistic cytoarchitectonic atlas (Bürgel et al., 2006) and the tractography-based probabilistic fiber atlas by Thiebaut de Schotten et al. (2011) defined at a probability of $p \geq 0.3$. Only structures with at least 100 mm^3 of overlapping voxels were reported in the table.

GM structure (AAL)	Number of voxels (mm^3)	β (Mean/SD)	β (Peak)
Middle temporal gyrus	8441	3.13/0.60	5.66
Inf. temporal gyrus	3078	2.59/0.57	4.40
Middle occipital gyrus	1677	3.37/0.61	5.73
Angular gyrus	1398	3.14/0.58	4.45
Sup. temporal gyrus	968	3.01/0.54	5.10
Pallidum	848	4.35/1.09	7.03
Middle frontal gyrus	739	2.62/0.53	4.73
Caudatum	719	3.24/0.63	5.72
Inf. frontal gyrus/triangular	706	2.23/0.23	3.99
Postcentral gyrus	570	2.92/0.35	4.17
Putamen	481	3.71/0.74	6.54
Rolandic operculum	422	3.74/0.53	5.22
Precentral gyrus	346	3.07/0.66	5.38
Inf. frontal gyrus/orbital	314	3.80/0.58	4.41
Amygdala	279	2.96/0.49	5.25
Supramarginal gyrus	228	2.88/0.35	3.73
Inf. occipital gyrus	214	3.45/0.95	5.23
Inf. parietal gyrus	166	2.81/0.24	3.68
Insula	119	3.00/0.93	5.99
Hippocampus	115	3.07/0.64	4.87
Sup. temporal pole	113	2.54/0.54	3.98
WM structure (Juelich)	**Number of voxels (mm^3)**	**β Mean/SD)**	**β (Peak)**
Callosal body	2703	4.10/1.09	7.31
Optic radiation	1393	3.07/0.67	5.48
Corticospinal tract	832	3.52/0.98	6.14
Sup. occipito-frontal fasciculus	262	4.26/0.91	6.84
Inf. occipito-frontal fasciculus	168	4.56/0.56	6.30
Uncinate fasciculus	134	4.36/0.68	6.30
WM structure (Thiebaut de Schotten)	**Number of voxels (mm^3)**	**β (Mean/SD)**	**β (Peak)**
Corpus callosum	3245	4.05/1.01	7.39
Internal capsule	2846	4.28/1.05	7.23
Inf. longitudinal fasciculus	2545	3.10/0.67	5.48
Arcuate fasciculus	2315	3.15/0.61	5.42
Posterior segment (Arcuate)	2036	3.07/0.58	4.88
Corticospinal tract	1845	4.19/1.07	7.23
Uncinate fasciculus	1249	3.26/0.82	6.30
Cingulum	1200	3.39/0.61	5.37
Anterior commissure	1177	3.21/0.85	5.88
Inf. occipito-frontal fasciculus	798	3.49/0.81	5.98
Optic radiations	306	3.37/0.66	5.42
Anterior segment (Arcuate)	282	3.71/0.57	5.42
Sup. longitudinal fasciculus	144	3.04/0.33	4.87

4. Discussion

The present study examined the lesion behavior relationship of spatial neglect in a newly recruited sample of right brain damaged patients. If the exact same methodological parameter configuration in terms of lesion volume correction and statistical thresholding (FDR correction and dTLVC for lesion size control) were used, both univariate as well as multivariate approaches revealed – in a single analysis – the same, complex network pattern underlying spatial neglect. At the cortical level, lesion location dominantly affected superior and middle temporal cortex and its borders into inferior parietal and occipital cortex. Beyond, parts of the insula and the inferior and middle frontal gyri were affected. Subcortically, we observed affection of parts of the pallidum, putamen and caudate nucleus as well as white matter fiber tracts, such as the superior and inferior longitudinal fasciculi, the superior and inferior occipito-frontal fasciculi, and the uncinate fasciculus. We further compared VLBM and MLBM methods by the predictive performance of both, the overall multivariate lesion behavior mapping model to the predictive performance of each individual voxel in univariate lesion behavior mapping after using dTLVC as lesion volume control procedure. This latter analysis showed that only few voxels were able to perform better than the combination of all voxels together in the multivariate model and that the predictive performance of the multivariate mapping technique was generally superior.

Despite the large sample size, the univariate analyses with lesion volume control by nuisance regression only detected one cluster in frontal white matter after FWE correction. A similar pattern was shown after using FDR correction with two small clusters in frontal white matter. Following results of these analysis, the univariate VLBM had enough power to generate a statistical map which was qualitatively comparable to the multivariate SVR-LSM map only when keeping residual signal of lesion size in the model. In the VLBM analysis including FWE correction, the univariate processing detected most of the regions that were also detected by the SVR-LSM analysis, with the exception of the inferior parietal lobule. The major difference was that VLBM detected massively less signal, resulting in only few actually interpretable clusters. In contrast, the VLBM analysis including FDR thresholding showed a more liberal pattern with a large number of detections. Some of these detections might not be directly linked to spatial neglect, but rather reflect areas with high lesion volume coverage, limiting the interpretation on the spatial extend of neglect behavior. Hence, it should be noted that the results of the latter two analyses were coupled to the omission of lesion volume control. However, since the severity of a behavioral symptom is often strongly correlated with total lesion volume and larger lesions are more likely to affect critical anatomical areas (Karnath et al., 2004), a form of correction is desired to detect the neural correlate specific to the behavioral symptom of interest. The comparison between the FDR thresholded statistical map without lesion volume control (Fig. 5C) and the average lesion volume plot (Fig. S3) revealed that the statistical topography might be biased towards areas with relatively large average lesion volumes. This impression could be quantitatively confirmed by a significant correlation between the unthresholded univariate statistical map – z-scores – without lesion volume correction and the lesion overlap plot ($r = 0.57$; $p < 0.001$). Please note that the correlation was also present for the unthresholded multivariate β-score map without lesion volume correction ($r = 0.31$; $p < 0.001$).

As expected, the regression technique suggested by DeMarco and Turkeltaub (2018) to control for lesion size turned out to be much more conservative with a worse model fit compared to the dTLVC procedure (Zhang et al., 2014). A comparison of the resulting statistical map (Supplementary Material; Fig. S5) to the patient overlap plot (Fig. 1) revealed that especially those areas with the highest lesion frequency across our entire sample were spared out. The regression technique suggested by DeMarco and Turkeltaub (2018) limited the 'searchlight' rather to the border areas of the space of interest. Hence, the regression based control for lesion size appears to generally reduce the amount of significant detections. Indeed, DeMarco and Turkeltaub (2018) noted in their discussion, that the cost of using this technique is a more conservative voxel-wise thresholding. The authors applied SVR-LSM in combination with their lesion volume regression approach on twenty real behavioral scores, but found significant results only in seven of these analyses. This further underlines that lesion volume control by regressing out lesion size from both behavioral and lesion scores, might be excessively conservative in many situations (including the present data). Results using this type of lesion size control thus should be interpreted with caution.

The simulations by Zhang et al. (2014) showed that SVR-LSM is characterized by a good receiver operator characteristic (ROC) performance, especially if lesion-volume correction by dTLVC is included. In

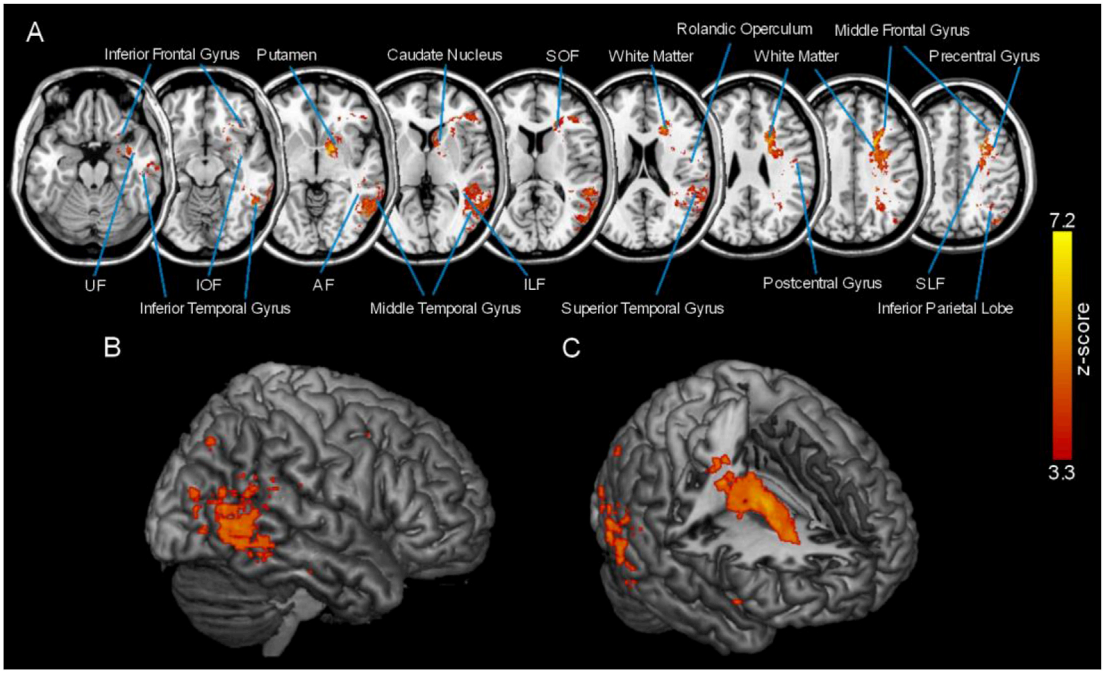

Fig. 4. Results of the univariate lesion behavior mapping using dTLVC. Mass-univariate lesion-symptom mapping results using data of 203 patients. Z-score maps are plotted for VLBM analysis with lesion volume correction by using dTLVC and FDR thresholded at $q = 0.05$, corresponding to a threshold of $z > 3.3828$. Significant clusters were interpreted according to the AAL atlas (Tzourio-Mazoyer et al., 2002) for grey matter regions and to the Juelich probabilistic cytoarchitectonic fiber tract atlas (Bürgel et al., 2006) as well as the tractography-based probabilistic fiber atlas by Thiebaut de Schotten et al. (2011) for white matter structures. B and C: three-dimensional renderings of the same map using the 3D-interpolation algorithm provided by MRIcron (http://people.cas.sc.edu/rorden/mricron/index.html; 8 mm search depth) with sagittal view for B and inside view for C. Results of A, B and C are shown as 1-p. D: Thresholded β-parameter map showing only significant areas according to A. Abbreviations: SLF – superior longitudinal fasciculus; AF – arcuate fasciculus; ILF – inferior longitudinal fasciculus; IOF – inferior occipitofrontal fasciculus; SOF – superior occipitofrontal fasciculus; UF – Uncinate fasciculus.

contrast, ROC characteristics of VLBM were generally worse and thresholds with both good sensitivity and specificity were not available. While Zhang et al. (2014) showed an overall superior performance of the multivariate mapping technique, it might be possible that, in the present investigation, the large sample size contributed to high power amongst various regions. To validate this assumption, it would be necessary to conduct a simulation study using different sample sizes and evaluate how this modification affects results of univariate and multivariate mapping.

Taking all of our univariate findings together, one can conclude that in the framework of multi-area based syndromes, VLBM does not in general fail to detect such networks. Rather, results in lesion symptom mapping can be influenced by the exact choice of analysis parameters (e.g. minimum lesion affection, lesion volume control procedure, and correction for multiple comparisons). In the present study, one of our various VLBM analyses used FDR correction and a very recent procedure for lesion size control, namely dTLVC. By using this type of univariate VLBM analysis, we obtained the same complex network pattern underlying spatial neglect as we revealed it by using a multivariate lesion analysis approach for the same data set. Whether this conclusion also applies to other cognitive deficits and data sets remains to be seen and will have to be investigated in future studies. For the moment, however, we suggest to apply dTLVC rather than the tradional nuisance regression procedure if using a univariate lesion analysis approach. For this purpose we integrated the dTLVC lesion volume correction into the NiiStat tool (https://github.com/neurolabusc/NiiStat) and hence this type of correction can now easily be applied by using this toolbox.

In contrast to our present MLBM findings, two previous multivariate examinations on spatial neglect (Smith et al., 2013; Toba et al., 2017) were able to uncover only parts of the discussed network. Very likely this is due to the small sample size in one of them (Toba et al., 2017) and – most importantly – the very limited number of a priori defined brain regions per multivariate model in both studies. In another recent multivariate investigation using ridge regression (Corbetta et al., 2015), the authors pointed to limitations based on sufficient lesion overlap in some areas which affects ridge regression performance. Hence, they were able to delineate only those parts of the network which were sufficiently sampled. In a similar way, Carter et al. (2017) used ridge regression and reduced their analysis a priori to the right middle cerebral artery territories for their multivariate mapping. In contrast, the present multivariate SVR-LSM analysis as well as our VLBM analysis using the same parameter configurations both utilized voxel-wise information and uncovered a larger set of cortical and subcortical areas, able to account for inconsistencies on the anatomical representation of spatial neglect. The finding highly corresponds to the areas proposed as being part of the 'perisylvian network' representing the anatomical basis for processes involved in spatial orienting and neglect (Karnath and Rorden, 2012), consisting of superior/middle temporal, inferior parietal, ventrolateral frontal cortices as well as their white matter connections. In that context, it is worth mentioning that our Fig. 3A bears a clear resemblance from Fig. 5A from Carter et al. (2017). Both studies have relatively large sample sizes (Carter et al., [2017] tested 70 individuals; the present study tested 203 patients) with continuous measures. However, it is also worth noting that both studies illustrate very different patient behaviors. While our present work directly measured neglected stimuli by using a conventional neglect cancellation task, Carter et al. (2017) used a reaction time measure where responses slower than 2000 ms were excluded. Therefore, the 'field effect' illustrated in their Fig. 5A illustrates slowed responses to perceived stimuli rather than the lack of responses due to truly neglected stimuli.

At the cortical level, lesion location dominantly affected the temporal

Table 3
Detailed overview of all significant grey and white matter clusters – VLBM. Overlap of VLBM analysis with control for lesion size by dTLVC with grey and white matter atlases: FDR correction at $q = 0.05$, corresponding to a threshold of $z > 3.3828$ **(A)**. Overlap of VLBM analysis without control for lesion size with grey and white matter atlases **(B & C). B:** permutation-based FWE correction at $p < 0.05$, corresponding to a threshold of $z > 5.3475$; **C:** FDR correction at $q = 0.05$, corresponding to a threshold of $z > 2.8607$. For grey matter structures, reports are generated using the Automatic Anatomical Labeling atlas (AAL; Tzourio-Mazoyer et al., 2002). For white matter structures, reports are generated using the Juelich probabilistic cytoarchitectonic atlas (Bürgel et al., 2006) and the tractography-based probabilistic fiber atlas by Thiebaut de Schotten et al. (2011) defined at a probability of $p \geq 0.3$. Only structures with at least 100 mm^3 of overlapping voxels were reported in the table. For the VLBM analyses with correction for lesion size, no overlap table is generated, as no clear labeling was possible.

A) FDR- thresholding with dTLVC correction

GM structure (AAL)	Number of voxels (mm^3)	z-score (Mean/SD)	z-score (Peak)
Middle temporal gyrus	7784	3.98/0.51	6.52
Inf. temporal gyrus	3141	4.21/0.56	6.43
Sup. temporal gyrus	1812	3.83/0.35	5.63
Middle. frontal gyrus	883	4.10/0.59	6.23
Angular gyrus	762	3.77/0.34	5.21
Inf. frontal gyrus/triangular	756	3.86/0.31	4.95
Middle occipital gyrus	614	3.85/0.41	5.62
Pallidum	568	4.49/0.89	6.86
Caudate	521	3.92/0.45	5.10
Inf. frontal gyrus/orbital	486	3.82/0.28	4.70
Precentral gyrus	379	3.91/0.44	5.77
Putamen	356	3.77/0.41	5.90
Amygdala	249	3.90/0.41	5.13
Rolandic operculum	188	3.60/0.21	4.43
Sup. temporal pole	181	3.79/0.28	4.67
Supramarginal gyrus	151	3.72/0.28	5.12
Middle temporal pole	146	3.79/0.31	4.98
Inf. occipital gyrus	143	3.93/0.46	5.53
WM structure (Juelich)	**Number of voxels (mm^3)**	**z-score (Mean/SD)**	**z-score (Peak)**
Callosal body	2785	4.44/0.81	7.20
Corticospinal tract	1001	4.04/0.59	6.18
Optic radiation	951	3.77/0.35	5.46
Sup. occipito-frontal fasciculus	236	4.00/0.53	5.60
Sup. Longitudinal fasciculus	120	3.84/0.48	5.47
WM structure (Thiebaut De Schotten)	**Number of voxels (mm^3)**	**z-score (Mean/SD)**	**z-score (Peak)**
Corpus callosum	2909	4.51/0.81	7.20
Internal capsule	2510	4.32/0.85	7.20
Arcuate fasciculus	2293	3.82/0.41	6.22
Posterior segment (Arcuate)	2090	3.84/0.42	6.22
Corticospinal tract	1676	4.27/0.76	6.84
Inf. longitudinal fasciculus	1550	3.85/0.42	6.43
Uncinate	1093	3.79/0.34	5.36
Anterior commissure	1019	4.18/0.72	6.86
Cingulate	916	4.28/0.59	6.25
Inf. occipito-frontal fasciculus	547	3.69/0.23	4.87
Optic radiations	303	3.72/0.27	4.73
Sup. longitudinal fasciculus	238	3.71/0.28	4.50
Anterior segment (Arcuate)	208	3.63/0.21	4.36

B) FWE- thresholding without correction for lesion size

GM structure (AAL)	Number of voxels (mm^3)	z-score (Mean/SD)	z-score (Peak)
Middle temporal gyrus	1304	5.66/0.28	6.86
Pallidum	523	5.93/0.48	7.26
Middle frontal gyrus	438	5.85/0.35	6.96
Inf. frontal gyrus/triangular	391	5.63/0.19	6.05
Putamen	228	5.66/0.33	6.94
Sup. temporal gyrus	167	5.58/0.20	6.23
Caudatum	129	5.57/0.19	6.20
Inf. frontal gyrus/orbital	113	5.60/0.20	6.06
Middle occipital gyrus	113	5.73/0.28	6.55

Table 3 (*continued*)

B) FWE- thresholding without correction for lesion size

WM structure (Juelich)	Number of voxels (mm^3)	z-score (Mean/SD)	z-score (Peak)
Callosal body	1832	6.07/0.53	7.66
Corticospinal tract	544	5.80/0.36	6.75
Sup. occipito-frontal fasciculus	128	5.78/0.37	6.90
WM structure (Thiebaut De Schotten)	**Number of voxels (mm^3)**	**z-score (Mean/SD)**	**z-score (Peak)**
Corpus callosum	2508	6.01/0.52	7.66
Internal capsule	2187	5.97/0.49	7.66
Corticospinal tract	1771	5.89/0.41	7.41
Cingulate	530	5.78/0.34	7.24
Anterior commissure	304	5.97/0.48	7.26
Arcuate fasciculus	269	5.63/0.28	6.58
Posterior segment (Arcuate)	267	5.63/0.28	6.58
Cortico ponto cerebellum	169	5.76/0.34	6.69
Uncinate	126	5.60/0.22	6.36
Inf. longitudinal fasciculus	122	5.63/0.29	6.68
Inf. occipito-frontal fasciculus	100	5.58/0.22	6.36

C) FDR- thresholding without correction for lesion size

GM structure (AAL)	Number of voxels (mm^3)	z-score (Mean/SD)	z-score (Peak)
Middle temporal gyrus	25761	4.03/0.73	6.86
Sup. temporal gyrus	14260	3.68/0.61	6.23
Angular gyrus	8455	3.65/0.52	5.86
Putamen	7628	4.02/0.65	6.94
Insula	7501	3.45/0.40	5.36
Middle occipital gyrus	6529	3.69/0.58	6.55
Inf. temporal gyrus	6374	4.00/0.72	6.72
Inf. frontal gyrus/triangular	5894	3.89/0.77	6.05
Caudatum	5335	4.18/0.59	6.20
Precentral gyrus	5335	3.72/0.64	6.85
Inf. frontal gyrus/opercular	5158	3.47/0.46	5.87
Middle frontal gyrus	5078	4.08/0.81	6.96
Rolandic operculum	4609	3.60/0.54	5.90
Inf. frontal gyrus/orbital	4433	4.02/0.58	6.06
Supramarginal gyrus	4196	3.36/0.40	5.68
Inf. parietal gyrus	2814	3.35/0.38	4.89
Postcentral gyrus	2776	3.31/0.35	5.19
Pallidum	2158	4.87/0.80	7.26
Sup. temporal pole	2123	3.42/0.47	5.61
Amygdala	1351	3.96/0.59	6.12
Hippocampus	1060	3.57/0.58	5.60
Sup. parietal gyrus	704	3.25/0.30	4.72
Thalamus	664	3.42/0.47	5.14
Middle temporal pole	601	3.54/0.53	5.47
Inf. occipital gyrus	392	4.12/0.83	6.50
Olfactory cortex	276	3.62/0.38	4.77
Sup. occipital gyrus	195	3.18/0.26	4.21
Fusiform gyrus	154	3.40/0.45	4.81
Transverse temporal gyrus	139	3.03/0.13	3.48
Sup. frontal gyrus/orbital	103	3.94/0.43	4.86
WM structure (Juelich)	**Number of voxels (mm^3)**	**z-score (Mean/SD)**	**z-score (Peak)**
Corticospinal tract	10278	3.90/0.76	6.75
Corpus callosum	8367	4.40/1.10	7.66
Optic radiation	7702	3.79/0.59	6.64
Sup. longitudinal fasciculus	1925	3.64/0.53	6.11
Inf. occipito-frontal fasciculus	1742	3.72/0.49	5.14
Sup. occipito-frontal fasciculus	1377	4.35/0.75	6.90
Acoustic radiation	794	3.32/0.36	4.68
Uncinate fasciculus	738	3.98/0.46	5.80
WM structure (Thiebaut De Schotten)	**Number of voxels (mm^3)**	**z-score (Mean/SD)**	**z-score (Peak)**
Internal capsule	16030	4.24/0.95	7.66
Arcuate fasciculus	15722	3.91/0.63	6.58
Corticospinal tract	11583	4.23/0.97	7.41
Inf. longitudinal fasciculus	10365	3.80/0.60	6.68
Posterior segment (Arcuate)	9743	4.07/0.65	6.58
Corpus callosum	9737	4.59/1.06	7.66
Inf. occipito-frontal fasciculus	9049	3.84/0.58	6.36

(*continued on next page*)

Table 3 (*continued*)

WM structure (Thiebaut De Schotten)	Number of voxels (mm^3)	z-score (Mean/SD)	z-score (Peak)
Uncinate fasciculus	6650	3.97/0.61	6.36
Anterior segment (Arcuate)	6335	3.63/0.48	5.47
Anterior commissure	3889	4.17/0.79	7.26
Optic radiations	2965	3.84/0.58	5.79
Cingulum	2914	4.38/0.92	7.24
Cortico ponto cerebellar	2607	3.78/0.80	6.69
Fornix	1208	3.47/0.44	5.18
Sup. longitudinal fasciculus	1205	3.78/0.52	5.35
Long segment (Arcuate)	691	3.58/0.44	5.02

cortex and its borders into inferior parietal and occipital cortices (cf. Figs. 3 and 4). The right temporal lobe has been delineated in previous lesion mapping studies in spatial neglect (Karnath et al., 2001, 2004; 2011; Committeri et al., 2007; Saj et al., 2012; Rousseaux et al., 2015). Smith et al. (2013) found the superior temporal gyrus (STG) as being the only structure which contained unique information for predicting spatial neglect. Accordingly, the STG seems to play an important role in multisensory integration, conveying information from both, the dorsal route of visual information processing, as well as polysensory inputs from the ventral perceptual stream (for review, see Karnath et al., 2001). Further evidence for the importance of superior/middle temporal areas for spatial neglect comes from recent animal models (Bogadhi et al., 2019). The authors detected a causal relationship between spatial neglect like symptoms and the superior temporal sulcus by direct and indirect 'inactivation' of that area in the monkey brain, underlining it's crucial role in covert attentional processing. In the human brain, the posterior part of the STG at the intersection to the inferior parietal cortex, an area which is called 'temporo-parietal junction' (TPJ) (Chang et al., 2013; Kincade et al., 2005; Macaluso and Doricchi, 2013) together with the ventral frontal cortex (VFC) (Corbetta and Shulman, 2002; Snyder and Chatterjee, 2006) have been reported as target areas for attentional reorienting, target detection and vigilance (Corbetta and Shulman, 2011). Lesions in these cortical areas, together with white matter disconnection hindering the information transmission between them (see below), seem to form the basis for the core deficit observed in spatial neglect patients.

The superior longitudinal fasciculus connects the ventral frontal cortex to parietal structures via different sub-branches, the SLF I, SLF II and SLF III, identified in both humans, and monkeys (Schmahmann and Pandya, 2006; Thiebaut de Schotten et al., 2011). The SLF has repeatedly been

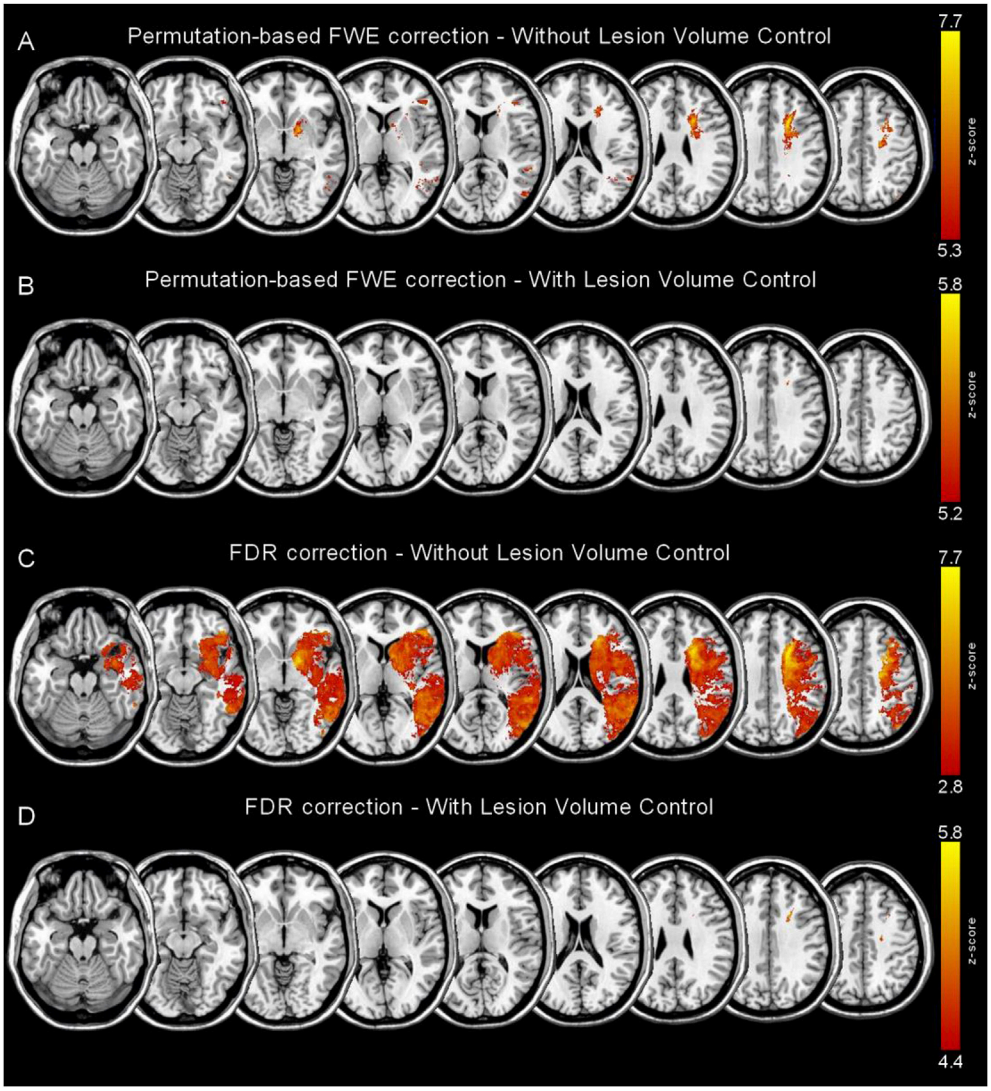

Fig. 5. Results of all further univariate lesion behavior mapping analyses. Mass-univariate lesion-symptom mapping results using data of 203 patients. Z-score maps are plotted for FWE permutation-thresholded as well as FDR-thresholded VLBM analyses with and without lesion volume correction on CoC scores. A: FWE permutation thresholded VLBM analysis without correction for lesion size at $p < 0.05$, corresponding to a threshold of $z > 5.3475$; B: FWE permutation thresholded VLBM analysis with correction for lesion size – by regressing lesion size out of behavior – at $p < 0.05$, corresponding to a threshold of $z > 5.2251$; C: FDR thresholded VLBM analysis without correction for lesion size at $q = 0.05$, corresponding to a threshold of $z > 2.8607$; D: FDR thresholded VLBM analysis with correction for lesion size – by regressing lesion size out of behavior – at $q = 0.05$, corresponding to a threshold of $z > 4.4772$.

discussed as being a crucial fronto-parietal pathway for processes of attentional orienting (Corbetta and Shulman, 2002; Bartolomeo et al., 2007). The ventral branch of the SLF (SLF III) specifically connects brain regions within the ventral attention network (VAN) (Rushworth et al., 2006; Bartolomeo et al., 2012; Thiebaut de Schotten et al., 2011) engaged in the propagation of information of stimulus identity and during the automatic capture of spatial attention by visual targets (Corbetta and Shulman, 2002). A further intrahemispheric tract partly overlapping with the SLF and confirmed in the present investigation is the arcuate fasciculus (AF). The AF is sometimes considered as an additional subcomponent of the SLF (Makris et al., 2005; Vernooij et al., 2007) and has been discussed in the transmission of information related to visuospatial performance (Chechlacz et al., 2014; Ciaraffa et al., 2013; Thiebaut De Schotten et al., 2014). This fiber bundle is composed of long and short anterior as well as short posterior fibers connecting specifically perisylvian frontal, parietal and temporal areas (Catani and Thiebaut de Schotten, 2008). Additionally, our results indicate the crucial involvement of the occipitofrontal fasciculus (IOF) – also termed as 'inferior frontooccipital fasciculus' (IFOF) –, which runs through the temporal lobe medial to the lower insula and connects areas of the frontal cortex with posterior temporal, inferior parietal, and occipital cortices (Nieuwenhuys et al., 1988; Catani et al., 2002; Bürgel et al., 2006; Forkel et al., 2014; Lawes et al., 2008). It has been suggested, that damage of this tract may hamper the transmission and/or the serial encoding of visual information in memory (Humphreys et al., 2015). This might explain deficits in target/distractor discriminative cancellation tasks, whereas no specific link between the IOF on line cancellation without distractor items has been reported (Urbanski et al., 2008). Our analysis depicted also the inferior longitudinal fasciculus (ILF), a further association tract connecting temporal to occipital areas (Catani et al., 2008), which has been linked previously to spatial neglect (Bird et al., 2006; Toba et al., 2018).

The present analysis also observed significant clusters subcortically for the right basal ganglia, including putamen, pallidum, and caudate nucleus. Based on previous work using perfusion imaging to monitor the remote effects of subcortical lesions (e.g. Hillis et al., 2002; Karnath et al., 2005), it is very likely that lesions of the basal ganglia lead to behavioral dysfunction by impairing the cortical network indirectly by malperfusion. However, there might also be a direct involvement of the basal ganglia. A recent simulation study by Parr and Friston (2018) aimed to formulate spatial neglect as a computational deficit. By setting up a model structure corresponding to the anatomy of dorsal and ventral attention networks, as well as their subcortical contributions, they demonstrated that basal ganglia lesions can directly produce neglect behavior in a saccadic cancellation task.

Interestingly, we also found significant clusters in areas and fibers typically associated with primary visual field defects (occipital gyri, optic radiation). Indeed, in our experiment, patients with visual field defects were not excluded from the analysis. The rationale for this follows two purposes. First, patients with visual field defects will probably have a more posterior lesion. Excluding such patients systematically from the analysis (or considering this as a co-variable of no interest) could produce an unwanted anatomical bias, namely an artificially created shift towards and increased power for detecting more anterior brain regions. Secondly, previous investigations have shown that visual field defects do not exacerbate neglect-specific symptoms in exploration tasks (e.g., Halligan et al., 1990). In agreement with such findings, the presence or absence of visual field defects was not significantly correlated with the patients' CoC scores ($r = 0.15$, n.s.). Finally, it might be possible that in a particular number of patients of our sample there is a co-occurrence of lesion patterns that alter a neglect-specific anatomical module but also spreading over to more posterior areas and fiber tracts associated with primary visual field defects. Thus, it is possible that in lesion mapping these areas will become significant although they are not directly involved in neglect behavior. This might also explain why the correlation between primary visual field defects and the CoC score was not significant and why we observed patients with primary visual field defects among those with as well as without spatial neglect.

Summarizing our anatomical results, multivariate and univariate lesion behavior mapping were able to depict the network by using only the CoC score as behavioral proxy for spatial neglect and attention, whereas previous studies have employed either a meta-analytical (Chechlacz et al., 2012; Molenberghs et al., 2012), multi-imaging/multi-method (Corbetta et al., 2015; Ramsey et al., 2016), or ROI approaches (Smith et al., 2013) to increase power or to disentangle the behavioral sub-functions and map them separately (Verdon et al., 2010; Vaessen et al., 2016; Toba et al., 2018) to come to comparable conclusions. This indicates that the behavioral proxy we measured here is indeed a core symptom of spatial neglect as it might evolve regardless where within this network a lesion produces focal dysfunction or remote deficits through disconnection. Nevertheless, we want to emphasize that future studies might apply the same analysis procedures used here for the core symptom of spatial neglect to uncover the neural underpinnings of the dissociating spatial and non-spatial behaviors. To disentangle the different components, these behavioral tasks in such future studies should be as fine graded as possible to detect a specific cognitive function in isolation (for discussion, see Sperber and Karnath, 2018; Vuilleumier, 2013; Saj et al., 2012).

5. Conclusion

The comparison between univariate and multivariate lesion analysis techniques revealed that spatial maps corresponded with each other if the exact same correction factors and parameter combinations (FDR correction and dTLVC for lesion size control) were used. Both approaches uncovered a complex network pattern underlying spatial neglect (though SVR-LSM was able to provide a better overall model fit throughout the statistically significant areas). Our findings underline the importance of a right network in spatial exploration and attention and specifically in the emergence of the core symptoms of spatial neglect. A remaining task for future studies is to investigate if the SVR-LSM approach employed here is indeed the most suitable multivariate analysis technique for studying the type of research question addressed in the present study. A comparison of different multivariate algorithms in multivariate lesion-behavior mapping as well as the evaluation of the impact of varying sample sizes in the comparison between univariate and multivariate mapping are needed.

Acknowledgments

This work was supported by the Deutsche Forschungsgemeinschaft (KA 1258/23–1) and National Institutes of Health (P50DC014664). Daniel Wiesen was supported by the Luxembourg National Research Fund (FNR/11601161); Christoph Sperber by the Friedrich Naumann Foundation.

Appendix A. Supplementary data

Supplementary data to this article can be found online at https://doi.org/10.1016/j.neuroimage.2019.07.013.

References

Azouvi, P., 2002. Sensitivity of clinical and behavioural tests of spatial neglect after right hemisphere stroke. J. Neurol. Neurosurg. Psychiatry 73, 160–166. https://doi.org/10.1136/jnnp.73.2.160.

Bartolomeo, P., Thiebaut de Schotten, M., Doricchi, F., 2007. Left unilateral neglect as a disconnection syndrome. Cerebr. Cortex 17, 2479–2490. https://doi.org/10.1093/cercor/bhl181.

Bartolomeo, P., Thiebaut de Schotten, M., Chica, A.B., 2012. Brain networks of visuospatial attention and their disruption in visual neglect. Front. Hum. Neurosci. 6, 1–10. https://doi.org/10.3389/fnhum.2012.00110.

Barton, J.J., Black, S.E., 1998. Line bisection in hemianopia. J. Neurol. Neurosurg. Psychiatry 64, 660–662. https://doi.org/10.1136/jnnp.66.1.121a.

Bates, E., Wilson, S.M., Saygin, A.P., Dick, F., Sereno, M.I., Knight, R.T., Dronkers, N.F., 2003. Voxel-based lesion–symptom mapping. Nat. Neurosci. 6, 448–450. https://doi.org/10.1038/nn1050.

Becker, E., Karnath, H.-O., 2010. Neuroimaging of eye position reveals spatial neglect. Brain 133, 909–914. https://doi.org/10.1093/brain/awq011.
Becker, E., Karnath, H.O., 2007. Incidence of visual extinction after left versus right hemisphere stroke. Stroke 38, 3172–3174. https://doi.org/10.1161/STROKEAHA.107.489096.
Benjamini, Y., Yekutieli, D., 2001. The control of the false discovery rate in multiple testing under dependency. Ann. Stat. 29, 1165–1188. https://doi.org/10.1214/aos/1013699998.
Binder, J., Marshall, R., Lazar, R., Benjamin, J., Mohr, J.P., 1992. Distinct syndromes of hemineglect. Arch. Neurol. 49, 1187–1194. https://doi.org/10.1001/archneur.1992.00530350109026.
Bird, C.M., 2006. Visual neglect after right posterior cerebral artery infarction. J. Neurol. Neurosurg. Psychiatry 77, 1008–1012. https://doi.org/10.1136/jnnp.2006.094417.
Bogadhi, A., Bollimunta, A., Leopold, D., Krauzlis, R., 2019. Spatial attention deficits are causally linked to an area in macaque temporal cortex. Curr. Biol. 29 (5), 726–736.
Bürgel, U., Amunts, K., Hoemke, L., Mohlberg, H., Gilsbach, J.M., Zilles, K., 2006. White matter fiber tracts of the human brain: three-dimensional mapping at microscopic resolution, topography and intersubject variability. Neuroimage 29, 1092–1105. https://doi.org/10.1016/j.neuroimage.2005.08.040.
Carter, A.R., McAvoy, M.P., Siegel, J.S., Hong, X., Astafiev, S.V., Rengachary, J., Zinn, K., Metcalf, N.V., Shulman, G.L., Corbetta, M., 2017. Differential white matter involvement associated with distinct visuospatial deficits after right hemisphere stroke. Cortex 88, 81–97. https://doi.org/10.1016/j.cortex.2016.12.009.
Catani, M., 2006. Diffusion tensor magnetic resonance imaging tractography in cognitive disorders. Curr. Opin. Neurol. 19, 599–606. https://doi.org/10.1097/01.wco.0000247610.44106.3f.
Catani, M., Howard, R.J., Pajevic, S., Jones, D.K., 2002. Virtual in vivo interactive dissection of white matter fasciculi in the human brain. NeuroImage 17, 77–94. https://doi.org/10.1006/nimg.2002.1136.
Catani, M., Thiebaut de Schotten, M., 2008. A diffusion tensor imaging tractography atlas for virtual in vivo dissections. Cortex 44, 1105–1132. https://doi.org/10.1016/j.cortex.2008.05.004.
Chang, C., Lin, C., 2013. LIBSVM : a library for support vector machines. ACM Trans. Intell. Syst. Technol. 2, 1–39. https://doi.org/10.1145/1961189.1961199.
Chang, C., Hsu, T., Tseng, P., Liang, W., Tzeng, O.J.L., Hung, D.L., Juan, C., 2013. Right temporoparietal junction and attentional reorienting. Hum. Brain Mapp. 877, 869–877. https://doi.org/10.1002/hbm.21476.
Chechlacz, M., Rotshtein, P., Bickerton, W.-L., Hansen, P.C., Deb, S., Humphreys, G.W., 2010. Separating neural correlates of allocentric and egocentric neglect: distinct cortical sites and common white matter disconnections. Cogn. Neuropsychol. 27, 277–303. https://doi.org/10.1080/02643294.2010.519699.
Chechlacz, M., Rotshtein, P., Humphreys, G.W., 2012. Neuroanatomical dissections of unilateral visual neglect symptoms: ALE meta-analysis of lesion-symptom mapping. Front. Hum. Neurosci. 6, 1–20. https://doi.org/10.3389/fnhum.2012.00230.
Chechlacz, M., Novick, A., Rotshtein, P., Bickerton, W.L., Humphreys, G.W., Demeyere, N., 2014. The neural substrates of drawing: a voxel-based morphometry analysis of constructional, hierarchical, and spatial representation deficits. J. Cogn. Neurosci. 26, 2701–2715.
Chen, Q., Middleton, E., Mirman, D., 2018. Words fail: lesion-symptom mapping of errors of omission in post-stroke aphasia. J. Neuropsychol. 1–15. https://doi.org/10.1111/jnp.12148.
Ciaraffa, F., Castelli, G., Parati, E.A., Bartolomeo, P., Bizzi, A., 2013. Visual neglect as a disconnection syndrome? A confirmatory case report. Neurocase 19, 351–359. https://doi.org/10.1080/13554794.2012.667130.
Committeri, G., Pitzalis, S., Galati, G., Patria, F., Pelle, G., Sabatini, U., Castriota-Scanderbeg, A., Piccardi, L., Guariglia, C., Pizzamiglio, L., 2007. Neural bases of personal and extrapersonal neglect in humans. Brain 130, 431–441. https://doi.org/10.1093/brain/awl265.
Corbetta, M., Shulman, G.L., 2002. Control of goal-directed and stimulus-driven attention in the brain. Nat. Rev. Neurosci. 3, 201–215. https://doi.org/10.1038/nrn755.
Corbetta, M., Kincade, M.J., Lewis, C., Snyder, A.Z., Sapir, A., 2005. Neural basis and recovery of spatial attention deficits in spatial neglect. Nat. Neurosci. 8, 1603–1610. https://doi.org/10.1038/nn1574.
Corbetta, M., Patel, G., Shulman, G.L., 2008. The reorienting system of the human brain: from environment to theory of mind. Neuron 58, 306–324. https://doi.org/10.1016/j.neuron.2008.04.017.
Corbetta, M., Shulman, G.L., 2011. Spatial neglect and attention networks. Annu. Rev. Neurosci. 34, 569–599. https://doi.org/10.1146/annurev-neuro-061010-113731.
Corbetta, M., Ramsey, L., Callejas, A., Baldassarre, A., Hacker, C.D., Siegel, J.S., Astafiev, S.V., Rengachary, J., Zinn, K., Lang, C.E., Connor, L.T., Fucetola, R., Strube, M., Carter, A.R., Shulman, G.L., 2015. Common behavioral clusters and subcortical anatomy in stroke. Neuron 85, 927–941. https://doi.org/10.1016/j.neuron.2015.02.027.
Cortes, C., Vapnik, V., 1995. Support-vector networks. Mach. Learn. 20, 273–297. https://doi.org/10.1023/A:1022627411411.
de Haan, B., Karnath, H.O., 2017. 'Whose atlas I use, his song I sing?' – the impact of anatomical atlases on fiber tract contributions to cognitive deficits after stroke. Neuroimage 163, 301–309. https://doi.org/10.1016/j.neuroimage.2017.09.051.
DeMarco, A.T., Turkeltaub, P.E., 2018. A multivariate lesion symptom mapping toolbox and examination of lesion-volume biases and correction methods in lesion-symptom mapping. Hum. Brain Mapp. 21, 2461–2467. https://doi.org/10.1002/hbm.24289.
Drucker, H., Burges, C.J.C., Kaufman, L., Smola, A., Vapnik, V., 1996. Support vector regression machines. Adv. Neural Inf. Process. Syst. 1, 155–161. https://www.doi.org/10.1.1.10.4845.
Fama, M.E., Hayward, W., Snider, S.F., Friedman, R.B., Turkeltaub, P.E., 2017. Subjective experience of inner speech in aphasia: preliminary behavioral relationships and neural correlates. Brain Lang. 164, 32–42. https://doi.org/10.1016/j.bandl.2016.09.009.
Ferber, S., Karnath, H.O., 2001. How to assess spatial neglect–line bisection or cancellation tasks? J. Clin. Exp. Neuropsychol. 23, 599–607. https://doi.org/10.1076/jcen.23.5.599.1243.
Forkel, S.J., Thiebaut de Schotten, M., Dell'Acqua, F., Danek, A., Catani, M., Williams, S.C.R., Catani, M., 2014. The anatomy of fronto-occipital connections from early blunt dissections to contemporary tractography. Cortex 56, 73–84. https://doi.org/10.1016/j.cortex.2012.09.005.
Fruhmann-Berger, M., Karnath, H.-O., 2005. Spontaneous eye and head position in patients with spatial neglect. J. Neurol. 252, 1194–1200. https://doi.org/10.1007/s00415-005-0831-y.
Fruhmann Berger, M., Proß, R., Ilg, U., Karnath, H.-O., 2006. Deviation of eyes and head in acute cerebral stroke. BMC Neurol. 6, 23. https://doi.org/10.1186/1471-2377-6-23.
Gajardo-Vidal, A., Lorca-Puls, D.L., Crinion, J.T., White, J., Seghier, M.L., Le, A.P., Hope, T.M.H., Ludersdorfer, P., Green, D.W., Bowman, H., Price, C.J., 2018. How distributed processing produces false negatives in voxel-based lesion-deficit analyses. Neuropsychologia 115, 124–133. https://doi.org/10.1016/j.neuropsychologia.2018.02.025.
Gauthier, Louise Dehaut, Francois Joanette, Y., 1989. The Bells Test: a quantitative and qualitative test for visual neglect. Int. J. Clin. Neuropsychol. 11, 49–54.
Griffis, J.C., Nenert, R., Allendorfer, J.B., Szaflarski, J.P., 2017a. Damage to white matter bottlenecks contributes to language impairments after left hemispheric stroke. Neuroimage: Clinical 14, 552–565. https://doi.org/10.1016/j.nicl.2017.02.019.
Griffis, J.C., Nenert, R., Allendorfer, J.B., Szaflarski, J.P., 2017b. Linking left hemispheric tissue preservation to fMRI language task activation in chronic stroke patients. Cortex 96, 1–18. https://doi.org/10.1016/j.cortex.2017.08.031.
Halligan, P.W., Marshall, J.C., Wade, D.T., 1990. Do visual field deficits exacerbate visuo-spatial neglect? Journal of Neurology Neurosurgery and Psychiatry 53, 487–491. https://doi.org/10.1136/jnnp.53.6.487.
He, B.J., Snyder, A.Z., Vincent, J.L., Epstein, A., Shulman, G.L., Corbetta, M., 2007. Breakdown of functional connectivity in frontoparietal networks underlies behavioral deficits in spatial neglect. Neuron 53, 905–918. https://doi.org/10.1016/j.neuron.2007.02.013.
Heilman, K.M., Watson, R.T., Valenstein, E., Damasio, A.R., 1983. Localization of lesions in neglect. In: Kertesz, A. (Ed.), Localization in Neuropsychology. Academic Press, New York, pp. 471–492.
Hillis, A.E., Wityk, R.J., Barker, P.B., Beauchamp, N.J., Gailloud, P., Murphy, K., Cooper, O., Metter, E.J., 2002. Subcortical aphasia and neglect in acute stroke: the role of cortical hypoperfusion. Brain 125, 1094–1104. https://doi.org/10.1093/brain/awf113.
Humphreys, G.W., Chechlacz, M., 2015. A neural decomposition of visual search using voxel-based morphometry. J. Cogn. Neurosci. 27, 1854–1869. https://doi.org/10.1162/jocn_a_00828.
Husain, M., Rorden, C., 2003. Non-spatially lateralized mechanisms in hemispatial neglect. Nat. Rev. Neurosci. 4, 26–36. https://doi.org/10.1038/nrn1005.
Husain, M., Shapiro, K., Martin, J., Kennard, C., 1997. Abnormal temporal dynamics of visual attention in spatial neglect patients. Nature. https://doi.org/10.1038/385154a0.
Karnath, H.-O., 2009. A right perisylvian neural network for human spatial orienting. In: Gazzaniga, M.S. (Ed.), The Cognitive Neurosciences IV. Mass.: MIT Press, Cambridge, pp. 259–268.
Karnath, H.-O., Ferber, S., Himmelbach, M., 2001. Spatial awareness is a function of the temporal not the posterior parietal lobe. Nature 411, 950–953. https://doi.org/10.1038/35082075.
Karnath, H.-O., Fruhmann Berger, M., Küker, W., Rorden, C., 2004. The anatomy of spatial neglect based on voxelwise statistical analysis: a study of 140 patients. Cerebr. Cortex 14, 1164–1172. https://doi.org/10.1093/cercor/bhh076.
Karnath, H.O., Rennig, J., Johannsen, L., Rorden, C., 2011. The anatomy underlying acute versus chronic spatial neglect: a longitudinal study. Brain 134, 903–912. https://doi.org/10.1093/brain/awq355.
Karnath, H.O., Rorden, C., 2012. The anatomy of spatial neglect. Neuropsychologia 50, 1010–1017. https://doi.org/10.1016/j.neuropsychologia.2011.06.027.
Karnath, H.O., Sperber, C., Rorden, C., 2018. Mapping human brain lesions and their functional consequences. Neuroimage 165, 180–189. https://doi.org/10.1016/j.neuroimage.2017.10.028.
Karnath, H.O., Zopf, R., Johannsen, L., Berger, M.F., Nägele, T., Klose, U., 2005. Normalized perfusion MRI to identify common areas of dysfunction: patients with basal ganglia neglect. Brain 128, 2462–2469. https://doi.org/10.1093/brain/awh629.
Kincade, J.M., 2005. An event-related functional magnetic resonance imaging study of voluntary and stimulus-driven orienting of attention. J. Neurosci. 25, 4593–4604. https://doi.org/10.1523/JNEUROSCI.0236-05.2005.
Lacey, E.H., Skipper-Kallal, L.M., Xing, S., Fama, M.E., Turkeltaub, P.E., 2017. Mapping common aphasia assessments to underlying cognitive processes and their neural substrates. Neurorehabilitation Neural Repair 31, 442–450. https://doi.org/10.1177/1545968316688797.
Lawes, I.N.C., Barrick, T.R., Murugam, V., Spierings, N., Evans, D.R., Song, M., Clark, C.A., 2008. Atlas-based segmentation of white matter tracts of the human brain using diffusion tensor tractography and comparison with classical dissection. Neuroimage 39, 62–79. https://doi.org/10.1016/j.neuroimage.2007.06.041.
Lorca-Puls, D.L., Gajardo-Vidal, A., White, J., Seghier, M.L., Leff, A.P., Green, D.W., Crinion, J.T., Ludersdorfer, P., Hope, T.M.H., Bowman, H., Price, C.J., 2018. The impact of sample size on the reproducibility of voxel-based lesion-deficit mappings. Neuropsychologia 115, 101–111. https://doi.org/10.1016/j.neuropsychologia.2018.03.014.

Lunven, M., Bartolomeo, P., 2017. Attention and spatial cognition: neural and anatomical substrates of visual neglect. Ann. Phys. Rehabil. Med. 60, 124–129. https://doi.org/10.1016/j.rehab.2016.01.004.
Macaluso, E., Doricchi, F., 2013. Attention and predictions: control of spatial attention beyond the endogenous-exogenous dichotomy. Front. Hum. Neurosci. 7, 75–80. https://doi.org/10.3389/fnhum.2013.00685.
Mah, Y.H., Husain, M., Rees, G., Nachev, P., 2014. Human brain lesion-deficit inference remapped. Brain 137, 2522–2531. https://doi.org/10.1093/brain/awu164.
Makris, N., Kennedy, D.N., McInerney, S., Sorensen, A.G., Wang, R., Caviness, V.S., Pandya, D.N., 2005. Segmentation of subcomponents within the superior longitudinal fascicle in humans: a quantitative, in vivo, DT-MRI study. Cerebr. Cortex 15, 854–869. https://doi.org/10.1093/cercor/bhh186.
McIntosh, R.D., Ietswaart, M., Milner, A.D., 2017. Weight and see: line bisection in neglect reliably measures the allocation of attention, but not the perception of length. Neuropsychologia 106, 146–158. https://doi.org/10.1016/j.neuropsychologia.2017.09.014.
Mesulam, M., 1981. A cortical network for directed attention and utlllateral neglect. Neurol. Prog. https://doi.org/10.1002/ana.410100402.
Molenberghs, P., Sale, M.V., Mattingley, J.B., 2012. Is there a critical lesion site for unilateral spatial neglect? A meta-analysis using activation likelihood estimation. Front. Hum. Neurosci. 6, 1–10. https://doi.org/10.3389/fnhum.2012.00078.
Nieuwenhuys, R., Voogd, J., van Huijzen, C., 1988. The Human Central Nervous System. Springer, Berlin.
Parr, T., Friston, K.J., 2018. The computational anatomy of visual neglect. Cerebr. Cortex 28, 777–790. https://doi.org/10.1093/cercor/bhx316.
Pustina, D., Avants, B., Faseyitan, O.K., Medaglia, J.D., Coslett, H.B., 2018. Improved accuracy of lesion to symptom mapping with multivariate sparse canonical correlations. Neuropsychologia 115, 154–166. https://doi.org/10.1016/j.neuropsychologia.2017.08.027.
Ramsey, L.E., Siegel, J.S., Baldassarre, A., Metcalf, N.V., Zinn, K., Shulman, G.L., Corbetta, M., 2016. Normalization of network connectivity in hemispatial neglect recovery. Ann. Neurol. 80, 127–141. https://doi.org/10.1002/ana.24690.
Rasmussen, P.M., Hansen, L.K., Madsen, K.H., Churchill, N.W., Strother, S.C., 2012. Model sparsity and brain pattern interpretation of classification models in neuroimaging. Pattern Recogn. 45, 2085–2100. https://doi.org/10.1016/j.patcog.2011.09.011.
Rorden, C., Bonilha, L., Fridriksson, J., Bender, B., Karnath, H.-O., 2012. Age-specific CT and MRI templates for spatial normalization. Neuroimage 61, 957–965. https://doi.org/10.1016/j.neuroimage.2012.03.020.
Rorden, C., Bonilha, L., Nichols, T.E., 2007. Rank-order versus mean based statistics for neuroimaging. Neuroimage 35, 1531–1537. https://doi.org/10.1016/j.neuroimage.2006.12.043.
Rorden, C., Fridriksson, J., Karnath, H.O., 2009. An evaluation of traditional and novel tools for lesion behavior mapping. Neuroimage 44, 1355–1362. https://doi.org/10.1016/j.neuroimage.2008.09.031.
Rorden, C., Karnath, H.O., 2010. A simple measure of neglect severity. Neuropsychologia 48, 2758–2763. https://doi.org/10.1016/j.neuropsychologia.2010.04.018.
Rousseaux, M., Allart, E., Bernati, T., Saj, A., 2015. Anatomical and psychometric relationships of behavioral neglect in daily living. Neuropsychologia 70, 64–70. https://doi.org/10.1016/j.neuropsychologia.2015.02.011.
Rushworth, M.F.S., Behrens, T.E.J., Johansen-Berg, H., 2006. Connection patterns distinguish 3 regions of human parietal cortex. Cerebr. Cortex 16, 1418–1430. https://doi.org/10.1093/cercor/bhj079.
Saj, A., Verdon, V., Vocat, R., Vuilleumier, P., 2012. "The anatomy underlying acute versus chronic spatial neglect" also depends on clinical tests. Brain 135, e207 e207. https://doi.org/10.1093/brain/awr227.
Sarri, M., Greenwood, R., Kalra, L., Driver, J., 2009. Task-related modulation of visual neglect in cancellation tasks. Neuropsychologia 47, 91–103. https://doi.org/10.1016/j.neuropsychologia.2008.08.020.
Schmahmann, J.D., Pandya, D.N., 2006. Fiber Pathways of the Brain. Oxford University Press, Oxford.
Shinoura, N., Suzuki, Y., Yamada, R., Tabei, Y., Saito, K., Yagi, K., 2009. Damage to the right superior longitudinal fasciculus in the inferior parietal lobe plays a role in spatial neglect. Neuropsychologia 47, 2600–2603. https://doi.org/10.1016/j.neuropsychologia.2009.05.010.
Skipper-Kallal, L.M., Lacey, E.H., Xing, S., Turkeltaub, P.E., 2017. Functional activation independently contributes to naming ability and relates to lesion site in post-stroke aphasia. Hum. Brain Mapp. 38 (4), 2051–2066. https://doi.org/10.1002/hbm.23504.
Smith, D.V., Clithero, J.A., Rorden, C., Karnath, H.-O., 2013. Decoding the anatomical network of spatial attention. Proc. Natl. Acad. Sci. U.S.A. 110, 1518–1523. https://doi.org/10.1073/pnas.1210126110.
Snyder, J.J., Chatterjee, A., 2006. The frontal cortex and exogenous attentional orienting. J. Cogn. Neurosci. 18, 1913–1923. https://doi.org/10.1162/jocn.2006.18.11.1913.
Sperber, C., Wiesen, D., Karnath, H.O., 2019. An empirical evaluation of multivariate lesion behaviour mapping. Hum. Brain Mapp.
Sperber, C., Karnath, H.-O., 2018. On the validity of lesion-behaviour mapping methods. Neuropsychologia 115, 17–24. https://doi.org/10.1016/j.neuropsychologia.2017.07.035.
Sperber, C., Karnath, H.O., 2016. Diagnostic validity of line bisection in the acute phase of stroke. Neuropsychologia 82, 200–204. https://doi.org/10.1016/j.neuropsychologia.2016.01.026.
Stone, S.P., Halligan, P.W., Greenwood, R., 1993. The incidence of neglect phenomena and related disorders in patients with an acute right or left hemisphere stroke. Age Ageing 22, 46–52. https://doi.org/10.1093/ageing/22.1.46.
Suchan, J., Karnath, H.O., 2011. Spatial orienting by left hemisphere language areas: a relict from the past? Brain 134, 3059–3070. https://doi.org/10.1093/brain/awr120.
Ten Brink, A.F., Verwer, J.H., Biesbroek, J.M., Visser-Meily, J.M.A., Nijboer, T.C.W., 2017. Differences between left- and right-sided neglect revisited: a large cohort study across multiple domains. J. Clin. Exp. Neuropsychol. 39, 707–723. https://doi.org/10.1080/13803395.2016.1262333.
Thiebaut de Schotten, M., ffytche, D.H., Bizzi, A., Dell'Acqua, F., Allin, M., Walshe, M., Murray, R., Williams, S.C., Murphy, D.G.M., Catani, M., 2011. Atlasing location, asymmetry and inter-subject variability of white matter tracts in the human brain with MR diffusion tractography. Neuroimage 54, 49–59. https://doi.org/10.1016/j.neuroimage.2010.07.055.
Thiebaut De Schotten, M., Tomaiuolo, F., Aiello, M., Merola, S., Silvetti, M., Lecce, F., Bartolomeo, P., Doricchi, F., 2014. Damage to white matter pathways in subacute and chronic spatial neglect: a group study and 2 single-case studies with complete virtual "in vivo" tractography dissection. Cerebr. Cortex 24, 691–706. https://doi.org/10.1093/cercor/bhs351.
Thiebaut de Schotten, M., Urbanski, M., Duffau, H., Volle, E., Lévy, R., Dubois, B., Bartolomeo, P., 2005. Direct evidence for a parietal-frontal pathway subserving spatial awareness in humans. Science 309, 2226–2228. https://doi.org/10.1126/science.1116251.
Toba, M.N., Zavaglia, M., Rastelli, F., Valabrégue, R., Pradat-Diehl, P., Valero-Cabré, A., Hilgetag, C.C., 2017. Game theoretical mapping of causal interactions underlying visuo-spatial attention in the human brain based on stroke lesions. Hum. Brain Mapp. 3471, 3454–3471. https://doi.org/10.1002/hbm.23601.
Toba, M.N., Migliaccio, R., Batrancourt, B., Bourlon, C., Duret, C., Pradat-Diehl, P., Dubois, B., Bartolomeo, P., 2018. Common brain networks for distinct deficits in visual neglect. A combined structural and tractography MRI approach. Neuropsychologia 115, 167–178. https://doi.org/10.1016/j.neuropsychologia.2017.10.018.
Tzourio-Mazoyer, N., Landeau, B., Papathanassiou, D., Crivello, F., Etard, O., Delcroix, N., Mazoyer, B., Joliot, M., 2002. Automated anatomical labeling of activations in SPM using a macroscopic anatomical parcellation of the MNI MRI single-subject brain. Neuroimage 15, 273–289. https://doi.org/10.1006/nimg.2001.0978.
Umarova, R.M., Reisert, M., Beier, T.U., Kiselev, V.G., Klöppel, S., Kaller, C.P., Glauche, V., Mader, I., Beume, L., Hennig, J., Weiller, C., 2014. Attention-network specific alterations of structural connectivity in the undamaged white matter in acute neglect. Hum. Brain Mapp. 35, 4678–4692. https://doi.org/10.1002/hbm.22503.
Urbanski, M., Thiebaut de Schotten, M., Rodrigo, S., Catani, M., Oppenheim, C., Touzé, E., Chokron, S., Méder, J.-F., Lévy, R., Dubois, B., Bartolomeo, P., 2008. Brain networks of spatial awareness: evidence from diffusion tensor imaging tractography. J. Neurol. Neurosurg. Psychiatry 79, 598–601. https://doi.org/10.1136/jnnp.2007.126276.
Urbanski, M., Thiebaut De Schotten, M., Rodrigo, S., Oppenheim, C., Touzé, E., Méder, J.F., Moreau, K., Loeper-Jeny, C., Dubois, B., Bartolomeo, P., 2011. DTI-MR tractography of white matter damage in stroke patients with neglect. Exp. Brain Res. 208, 491–505. https://doi.org/10.1007/s00221-010-2496-8.
Vaessen, M.J., Saj, A., Lovblad, K.O., Gschwind, M., Vuilleumier, P., 2016. Structural white-matter connections mediating distinct behavioral components of spatial neglect in right brain-damaged patients. Cortex 77, 54–68. https://doi.org/10.1016/j.cortex.2015.12.008.
Vapnik, V.N., 1995. The Nature of Statistical Learning Theory. Springer New York, New York, NY. https://doi.org/10.1007/978-1-4757-2440-0.
Verdon, V., Schwartz, S., Lovblad, K.-O., Hauert, C.-A., Vuilleumier, P., 2010. Neuroanatomy of hemispatial neglect and its functional components: a study using voxel-based lesion-symptom mapping. Brain 133, 880–894. https://doi.org/10.1093/brain/awp305.
Vernooij, M.W., Smits, M., Wielopolski, P.A., Houston, G.C., Krestin, G.P., van der Lugt, A., 2007. Fiber density asymmetry of the arcuate fasciculus in relation to functional hemispheric language lateralization in both right- and left-handed healthy subjects: a combined fMRI and DTI study. Neuroimage 35, 1064–1076. https://doi.org/10.1016/j.neuroimage.2006.12.041.
Vuilleumier, P., 2013. Mapping the functional neuroanatomy of spatial neglect and human parietal lobe functions: progress and challenges. Ann. N. Y. Acad. Sci. 1296, 50–74. https://doi.org/10.1111/nyas.12161.
Watson, R.T., Heilman, K.M., Miller, B.D., King, F.A., 1974. Neglect after mesencephalic reticular formation lesions. Neurology 24, 294–298.
Weintraub, S., Mesulam, M.-M., 1985. Mental state assessment of young and elderly adults in behavioral neurology. In: Mesulam, M.-M. (Ed.), Principles of Behavioral Neurology. F.A. Davis Company, Philadelphia, pp. 71–123.
Xing, S., Lacey, E.H., Skipper-Kallal, L.M., Jiang, X., Harris-Love, M.L., Zeng, J., Turkeltaub, P.E., 2016. Right hemisphere grey matter structure and language outcomes in chronic left hemisphere stroke. Brain 139 (1), 227–241. https://doi.org/10.1093/brain/awv323.
Yourganov, G., Smith, K.G., Fridriksson, J., Rorden, C., 2015. Predicting aphasia type from brain damage measured with structural MRI. Cortex 73, 203–215. https://doi.org/10.1016/j.cortex.2015.09.005.
Zavaglia, M., Hilgetag, C.C., 2016. Causal functional contributions and interactions in the attention network of the brain: an objective multi-perturbation analysis. Brain Struct. Funct. 221, 2553–2568. https://doi.org/10.1007/s00429-015-1058-z.
Zhao, L., Biesbroek, J.M., Shi, L., Liu, W., Kuijf, H.J., Chu, W.W.C., Wong, A., 2018. Strategic infarct location for post-stroke cognitive impairment: a multivariate lesion-symptom mapping study. J. Cereb. Blood Flow Metab. 38 (8), 1299–1311. https://doi.org/10.1177/0271678X17728162.
Zhang, Y., Kimberg, D.Y., Coslett, H.B., Schwartz, M.F., Wang, Z., 2014. Multivariate lesion-symptom mapping using support vector regression. Hum. Brain Mapp. 35, 5861–5876. https://doi.org/10.1002/hbm.22590.